The First Carbonyl Bond Dissociation Energies of $M(CO)_5$ and $M(CO)_4(C_2H_2)$ (M = Fe, Ru, and Os): The Role of the Acetylene Ligand from a Density Functional Perspective

Stephen A. Decker and Mariusz Klobukowski*

Contribution from the Department of Chemistry, University of Alberta, Edmonton, Alberta T6G 2G2, Canada

Received April 9, 1998. Revised Manuscript Received July 9, 1998

Abstract: Recent kinetics experiments have shown that the rate of carbonyl substitution in complexes of the type $M(CO)_4(C_2R_2)$, where M = Fe, Ru, and Os, is accelerated by factors of 10^2-10^{13} over their respective pentacarbonyl complexes. These substitution reactions have been shown to be dissociative in nature and show a marked metal dependence of the rate. The origin of the increased reactivity of these alkyne complexes was studied with nonlocal density functional theory (BLYP functional), using both effective core potential (ECP) and all-electron basis sets, in conjunction with Frenking's charge decomposition analysis (CDA) scheme and Bader's atoms in molecules (AIM) analysis. We found that the BLYP/ECP method predicted geometries very close to experiment for both the parent carbonyl and alkyne complexes (in this study C_2H_2 was used). The calculated CO bond dissociation energies (BDEs) were also found to agree well with experiment and mirrored the metal dependence trends observed experimentally for both $M(CO)_5$ and $M(CO)_4(C_2H_2)$. By using the CDA scheme the nature of the acetylene ligand was characterized in both the reactant, $M(CO)_4(C_2H_2)$, and the unsaturated dissociation product, $M(CO)_3(C_2H_2)$: acetylene was found to act as a two-electron donor in the reactant complex (with only the $\pi_{||}$ orbitals of C_2H_2 actively donating to the metal) and as a four-electron donor (with both the $\pi_{||}$ and the $\pi_{\perp}$ orbitals of C_2H_2 actively donating to the metal), increasing the stability of the otherwise 16-electron unsaturated dissociation product. The predicted structural changes along with the results of the AIM analysis fully support the CDA findings. At the BLYP/ECP level the observed rate enhancement compared to the parent $M(CO)_5$ compounds was rationalized in terms of the metal dependence of the molecular orbital energy gap for the $\pi_{\perp}$ $C_2H_2 \rightarrow M$ interaction, in the unsaturated $M(CO)_3(C_2H_2)$ intermediate.

1. Introduction

Transition metal carbonyls are among the best known and most widely studied organometallic complexes.[1] They are commonly used as starting materials in organometallic syntheses, and as catalytic precursors. However, they are typically saturated 18-electron species, and thus relatively inert.[2] It has been known for some time that certain spectator ligands in a metal complex can facilitate, either sterically or electronically, dissociation of CO. Numerous papers have demonstrated that when the ancillary ligand is a π-donor ligand, such as a halide, acetate, or chelating amido group, then the carbonyl ligand in the cis position tends to be labilized. This effect, known as cis labilization, has been observed and studied extensively through solution kinetics in d^6 (Cr, W) and d^7 (Mn, Re) complexes of the type $M(CO)_3\widehat{L\ L})^{2-}$ and $M(CO)_5$.[3] The proposed rationalization of this effect involves a stabilization of the dissociative unsaturated 16-electron transition state via π-donation from the ancillary ligand. This hypothesis has been supported in theoretical studies by Lichtenberger and Brown[4] (with the Fenske−Hall method) and Davy and Hall[5] (at the RHF level of theory), and the importance of π stabilization has recently been reviewed by Caulton.[6]

Recently Takats and Jordan[7,8] demonstrated that the presence of an η^2-alkyne ligand accelerates simple CO substitution reactions in complexes of the type $M(CO)_4(\eta^2$-alkyne), where the metal is a member of the iron triad and the alkyne is hexafluorobut-2-yne or acetylene. X-ray crystal structures of $Ru(CO)_4[C_2(CF_3)_2]$ and $Os(CO)_4[C_2(CF_3)_2]$ revealed trigonal bipyramid structures for the complexes, with the alkyne ligand occupying an in-plane equatorial site.[9] The kinetics of the

(1) (a) Schutzenberger, P. *Comptes Rendus* **1870**, *70*, 1134. (b) Mond, L.; Langer, C.; Quincke, F. *J. Chem. Soc.* **1890**, 749. (c) Abel, E. *J. Organomet. Chem.* **1990**, *383*, 11. (d) Herrmann, W. A. *J. Organomet. Chem.* **1990**, *383*, 21. (e) Werner, H. *Angew. Chem., Int. Ed. Engl.* **1990**, *29*, 1077.

(2) Collman, J. P.; Hegedus, L. S.; Norton, J. R.; Finke, R. G. *Principles and Applications of Organotransition Metal Chemistry*; University Science Books: Mill Valley, 1987.

(3) (a) Atwood, J. D.; Brown, T. L. *J. Am. Chem. Soc.* **1976**, *98*, 3160. (b) Cohen, M. A.; Brown, T. L. *Inorg. Chem.* **1976**, *15*, 1417. (c) Cotton, F. A.; Darensbourg, D. J.; Koltzhammer, B. W. S.; Kudaroski, R. *Inorg. Chem.* **1982**, *21*, 1656. (d) Darensbourg, D. J.; Klausmeyer, K. K.; Reibenspies, J. H. *Inorg. Chem.* **1995**, *34*, 4933. (e) Darensbourg, D. J.; Klausmeyer, K. K.; Reibenspies, J. H. *Inorg. Chem.* **1996**, *35*, 1529. (f) Darensbourg, D. J.; Klausmeyer, K. K.; Reibenspies, J. H. *Inorg. Chem.* **1996**, *35*, 1535.

(4) Lichtenberger, D. L.; Brown, T. L. *J. Am. Chem. Soc.* **1978**, *100*, 366.

(5) Davy, R. D.; Hall, M. B. *Inorg. Chem.* **1989**, *28*, 3524.

(6) Caulton, K. G. *New J. Chem.* **1994**, *18*, 25.

(7) Pearson, J.; Cooke, J.; Takats, J.; Jordan, R. B. *J. Am. Chem. Soc.* **1998**, *120*, 1434.

(8) Mao, T.; Zhang, Z.; Washington, J.; Takats, J.; Jordan, R. B. Manuscript in preparation.

(9) Marinelli, G.; Streib, W. E.; Huffman, J. C.; Caulton, K. G.; Gagne, M. R.; Takats, J.; Dartiguenave, M.; Chardon, C.; Jackson, S. A.; Eisenstein, O. *Polyhedron* **1990**, *9*, 1867.

S0002-7863(98)01197-4 CCC: $15.00
Published on Web 09/01/1998

carbonyl substitution process, with phosphines or phosphites, was monitored with IR spectroscopy. It was determined that when the alkyne was hexafluorobutyne (HFB), the phosphine/phosphite occupies an axial position (cis to the alkyne) in the monosubstituted product while both the axial positions are occupied by phosphine/phosphite groups in the disubstituted product. No further carbonyl substitution was observed beyond the disubstituted species in the HFB complexes.[7] Synthetic studies of the acetylene complex of Os have indicated that the substitution of a second phosphine leads to both the expected disubstituted product along with a number of acyl complexes, in which a CO ligand has inserted into the acetylene.[8]

All of the carbonyl substitution reaction rates were found to be independent of the nature and concentration of the incoming phosphine/phosphite group. This result, coupled with the positive value of $\Delta S^{\ddagger}$, led to the conclusion that the carbonyl substitution proceeds via a dissociative mechanism, in which the rate-determining step corresponds to loss of CO from $M(CO)_4(\eta^2$-alkyne) leading to the monosubstituted product. Comparison of the dissociation rate constants for these alkyne-substituted species with that of their respective parent carbonyls, $M(CO)_5$, indicated that the presence of the alkyne ligand has a profound influence. The rate constants for CO dissociation from the HFB complexes were found to be 3×10^{13} (Fe), 2×10^2 (Ru), and 1×10^7 (Os) faster than those of the corresponding pentacarbonyl complexes. The kinetics data also showed that it is the lowering of $\Delta H^{\ddagger}$ by 3−19 kcal/mol in the alkyne complexes relative to the pentacarbonyls that is responsible for the observed increased reactivity.[7]

To account for the increased reactivity of the alkyne complexes either (1) a ground-state destabilization effect or (2) a transition state stabilization effect may be invoked. According to Takats and Jordan,[7] there appear to be no significant geometric or spectroscopic differences between the $M(CO)_4(C_2(CF_3)_2)$ and $M(CO)_5$ reactant complexes to account for the increased CO lability. Hence, it was postulated that the increased CO lability must be due to stabilization of the dissociative 16-electron transition state, via increased π-donation from the alkyne ligand through participation of its π orbital perpendicular to the equatorial plane, in the direction of the vacated site. The variable electron donor ability of alkyne ligands in transition metal complexes, from two to four electrons, has been well documented.[10] For example, Templeton and Ward[11] have shown that ^{13}C NMR can be used to gauge the number of electrons formally donated by the alkyne to the metal.

The present computational study was undertaken to provide computational support for the role of the alkyne in enhancing CO substitution rates in $M(CO)_4(\eta^2$-alkyne) complexes. Although numerous theoretical papers have focused on the transition metal carbonyls, as illustrated in the review article of Veillard,[12] far fewer have centered on alkyne complexes. The bonding between acetylene and a naked metal atom (or cation) has been analyzed in several studies. For example, Mitchell et al.[13] probed the bonding between Ni and acetylene, using nonlocal density functional theory (DFT). Bauschlicher et al.[14] examined the bonding between acetylene and the cations of the first- and second-row transition series, using modified coupled-pair functional (MCPF) theory. Siegbahn[15] studied the C−H activation of acetylene by bare second-row transition metal atoms, at the CISD level of theory. Sellers[16] modeled the binding of acetylene to the Pd(111) surface at the MP2 level. Perhaps most relevant to the present study are the reports from the groups of Geurts, Frenking, and Morokuma which have examined aspects of the metal−acetylene bond in various transition metal complexes. Geurts et al.[17] examined the bonding between acetylene and Ni, in $Ni(CO)_2(C_2H_2)$, $Ni(CNH)_2(C_2H_2)$, and $Ni_2(CNH)_4(\mu_2\text{-}C_2H_2)$, at the Hartree−Fock−Slater local spin density level of theory. The transformation of coordinated η^2-acetylene to its vinylidene isomer in the Ru(II) complex, $Ru(PH_3)_2Cl_2(C_2H_2)$, and the Rh(I) complexes, $Rh(PH_3)_2Cl(C_2H_2)$ and $Rh(P^iPr_3)_2(Cl)(C_2H_2)$, was studied by Morokuma and co-workers[18] using the MP2 and IMOMM (MP2+MM3) methods. Frenking et al.,[19−22] using their recently developed charge decomposition analysis (CDA) scheme, probed the nature of the metal−acetylene bond in complexes of the type $MX_4(C_2H_2)$, $MX_5(C_2H_2)^-$, and $M(CO)_5(C_2H_2)$, where M = Cr, Mo, and W and X = F and Cl. To our knowledge there are no theoretical papers which focus specifically on the d^8 $M(CO)_4(C_2R_2)$ complexes of the iron triad studied experimentally by Takats and Jordan.[7]

2. Computational Methods

In the present study we focus on the rate determining dissociative loss of CO from the alkyne complexes and the parent pentacarbonyls. We employed nonlocal, gradient corrected density functional theory in conjunction with Frenking's charge decomposition analysis scheme[23] and Bader's atoms in molecules (AIM)[24,25] topological analysis of the electron density to probe the origins of the increased reactivity of the alkyne-substituted complexes.

To reduce the computational complexity of the present DFT calculations, acetylene was chosen as a model of the hexafluorobut-2-yne alkyne ligand used in the kinetics study. A recent kinetics study involving the Os alkyne complexes[8] showed that changing the alkyne ligand from hexafluorobut-2-yne to acetylene resulted in only a minor reduction in the value of $\Delta H^{\ddagger}$ for the CO dissociation from 23.8 kcal/mol to 21.8 kcal/mol. We trust that the simplified acetylene model complex used in our calculations will not hinder comparison to the experimental hexafluorobut-2-yne complexes.

For this class of molecules, both relativistic effects and electron correlation effects are very important. Relativistic effects were indirectly incorporated into our calculations through the use of quasirelativistic effective core potentials which have been derived from relativistic atomic calculations. Electron correlation is included in the density functional methodology through the correlation functional. The methods which incorporate electron correlation effects are always linked to the choice of basis set.[26] As clearly illustrated in our previous work on carbonyl migration in $Mn_2(CO)_{10}$, DFT exhibits a much faster basis

(10) Crabtree, R. H. *The Organometallic Chemistry of the Transtion Metals*; John Wiley and Sons: New York, 1988.
(11) Templeton, J. L.; Ward, B. C. *J. Am. Chem. Soc.* **1980**, *102*, 3288.
(12) Veillard, A. *Chem. Rev.* **1991**, *91*, 743.
(13) Mitchell, S. A.; Blitz, M. A.; Fournier, R. *Can. J. Chem.* **1994**, *72*, 587.
(14) Sodupe, M.; Bauschlicher, C. W., Jr. *J. Phys. Chem.* **1991**, *95*, 8640.
(15) Siegbahn, P. E. M. *Theor. Chim. Acta* **1994**, *87*, 277.
(16) Sellers, H. *J. Phys. Chem.* **1990**, *94*, 8329.
(17) Guerts, P.; Burgers, H.; van der Avoird, A. *Chem. Phys.* **1981**, *54*, 397.
(18) (a) Wakatsuki, Y.; Koga, N.; Yamazaki, H.; Morokuma, K. *J. Am. Chem. Soc.* **1994**, *116*, 8105. (b) Wakatsuki, Y.; Koga, N.; Werner, H.; Morokuma, K. *J. Am. Chem. Soc.* **1997**, *119*, 360.
(19) Stegmann, R.; Neuhaus, A.; Frenking, G. *J. Am. Chem. Soc.* **1993**, *115*, 11930.
(20) Pidun, U.; Frenking, G. *J. Organomet. Chem.* **1996**, *525*, 269.
(21) Ehlers, A. W.; Dapprich, S.; Vyboishchikov; Frenking, G. *Organometallics* **1996**, *15*, 105.
(22) Frenking, G.; Pidun, U. *J. Chem. Soc., Dalton Trans.* **1997**, 1653.
(23) Dapprich, S.; Frenking, G. *J. Phys. Chem.* **1995**, *99*, 9352.
(24) (a) Bader, R. F. W.; Tal, Y.; Anderson, S. G.; Nguyen-Dang T. T. *Isr. J. Chem.* **1980**, *19*, 8. (b) Bader, R. F. W.; Nguyen-Dang T. T. *Adv. Quantum Chem.* **1981**, *14*, 63. (c) Bader, R. F. W.; Nguyen-Dang T. T.; Tal, Y. *Rep. Prog. Phys.* **1981**, *44*, 893. (d) Bader, R. F. W.; Essén, H. *J. Chem. Phys.* **1984**, *80*, 1943.
(25) Bader, R. F. W. *Atoms in Molecules: A Quantum Theory*; Clarendon Press: Oxford, 1990.
(26) Shavitt, I. In *Methods of Electronic Structure Theory*; Schaefer, H. F., III, Ed.; Plenum: New York, 1977; p 243.

set convergence than correlated wave function methods, such as MP2 and CISD.[27] The DFT and HF-SCF total energies of the CO molecule are converged with only two d-type and one f-type polarization functions added to the atomic basis sets, while the correlated wave function methods remained unconverged even at the 3d 2f 1g level of polarization. Density functional calculations, converging in total energy as fast as SCF calculations do, require less care in basis set selection (and smaller expansions) than MP2 or CI calculations. Agreement with experiment obtained with MP2 or CI using small basis sets may be fortuitous, whereas the same basis sets may be adequate for securing converged results at the SCF and DFT levels of theory.

The primary basis set employed in the present study, denoted BS1, consists of the effective core potential (ECP) basis set of Stevens et al.[28] with a slight modification of the valence space to triple-ζ quality for the main group elements and quadruple-ζ quality for the metals. The basis was augmented with a single d polarization function on C and O, and a single p polarization function on H, all of which were taken from Huzinaga et al.[29] For the metal atoms a total of 16 electrons were included in the valence space, with a contracted Gaussian basis set of triple-ζ valence quality for the s and p space, and of quadruple-ζ valence quality for the d space. The overall contraction for Fe is (4211/4211/3111), while for Ru and Os it is (4111/4111/2111). The valence electrons of C and O were described by using a triple-ζ valence basis set with a (211/211/1*) contraction. The 4-31G basis set[30] augmented with a p polarization function was used for the H atoms. To probe the metal−acetylene bonding with the CDA[23] and AIM[24,25] schemes the all-electron double-ζ plus polarization basis sets of Salahub et al.[31] were used and denoted BS2. In the BS2 basis set Fe and Ru have contraction schemes of (63321/531/41) and (633321/53211/531), respectively (there was no basis set available for Os), while C and O have a (621/41/1*) contraction and H has a (41) contraction. It was necessary to replace the ECP basis set (BS1) with the all-electron basis set (BS2) because the AIM module as contained within the Gaussian94 package[32] is limited to all electron basis sets. In addition, we found the results of the CDA scheme to be rather sensitive to the choice of basis set. (Details will be discussed later.)

A variety of different functionals were employed in the DFT calculations. The primary functional used in our calculations was the BLYP functional, comprised of Becke's gradient-corrected exchange functional[33] in conjunction with the gradient-corrected correlation functional of Lee, Yang, and Parr.[34] This functional was used in all geometry optimizations and subsequent Hessian calculations, as well as for determination of the CO bond dissociation energies (BDEs), the CO dissociation trajectories, and the CDA and AIM analyses. The BP86 (Becke's nonlocal exchange functional[33] coupled with Perdew's nonlocal correlation functional[35]), B3LYP (Becke's three-parameter hybrid gradient-corrected exchange functional,[36] Becke3, coupled with the gradient-corrected correlation functional of Lee, Yang, and Parr[34]), and B3PW91 (Becke3 functional,[36] coupled with Perdew and Wang's nonlocal correlation functional[37]) functionals were employed to calculate the CO BDEs of the alkyne and parent carbonyl complexes from total energy differences at the respective BLYP optimized geometries. To test the validity of the assumption that the BLYP potential energy surface minima closely resemble those which would be obtained with other functionals, the geometries of several reactant and CO dissociation product complexes were optimized with the B3LYP functional and the resulting CO BDE determined. In all cases optimization of the geometries with the B3LYP functional resulted in no significant differences in the values of the CO BDEs when compared to those values obtained with the BLYP optimized geometries.

All geometries were optimized by using analytical gradient techniques and the stationary points characterized by harmonic vibrational analysis, accomplished via numerical differentiation of the analytical first derivatives. The zero point energy corrections from the harmonic vibrational frequencies were included in the CO BDE determinations, for the BLYP functional only.

The Gaussian94 program[32] was used throughout the study for all single point energy calculations, geometry optimizations, and hessian calculations, as well as for Bader's AIM analysis. The CDA2.1 program,[38] was used in conjunction with the standard output of the Gaussian92 package[39] to analyze the metal−acetylene bonding within the CDA scheme.

3. Results and Discussion

A. Structures of the Carbonyl Complexes. To calculate the first carbonyl BDE one must determine the total energies of the reactant complex, $M(CO)_5$, and the CO dissociated products, $M(CO)_4$ and CO. Hence, the first step involved optimization of their respective geometries to obtain the lowest-energy conformation in the ground electronic state.

1. $M(CO)_5$. In the gas phase the saturated metal pentacarbonyls exhibit a D_{3h} trigonal bipyramidal structure,[40−44] and as such they were optimized under D_{3h} symmetry at the BLYP/BS1 level of theory. The corresponding optimized geometric parameters are given in Table 1, and compared with experiment and the results of previous theoretical studies. To allow for a comparison of the effects of different functionals, the Ru and Os analogues were optimized with the B3LYP/BS1 method, and the results are also presented in Table 1.

Comparison of the calculated BLYP/BS1 structural parameters and the experimental gas-phase diffraction values shows that the level of theory used here yields quite accurate geometries, with average deviations of the M−C and C−O bond lengths of 0.014, 0.042, and 0.030 Å for the Fe, Ru, and Os analogues, respectively. The BLYP/BS1 method consistently overestimates both the M−C and C−O bonds in all of the complexes. While the B3LYP/BS1 method still overestimates the M−C and C−O distances, the overall agreement with experiment is slightly improved, with average deviations of 0.031 and 0.026 Å for the bond lengths of the Ru and Os analogues, respectively.

(27) Decker, S. A.; Donini, O.; Klobukowski, M. *J. Phys. Chem. A* **1997**, *101*, 8734.
(28) (a) Stevens, W. J.; Basch; H.; Krauss, M. *J. Chem. Phys.* **1984**, *81*, 6026. (b) Stevens, W. J.; Basch; H.; Krauss, M.; Jasien, P. *Can. J. Chem.* **1992**, *70*, 612. (c) Cundari, T. R.; Stevens, W. J. *J. Chem. Phys.* **1993**, *98*, 5555.
(29) Huzinaga, S., Ed. *Gaussian Basis Sets for Molecular Calculations*; Elsevier: Amsterdam, 1984.
(30) Ditchfield, R.; Hehre, W. J.; Pople, J. A. *J. Chem. Phys.* **1971**, *54*, 724.
(31) Godbout, N.; Salahub, D. R.; Andzelm, J.; Wimmer, E. *Can. J. Chem.* **1992**, *70*, 560.
(32) GAUSSIAN 94, Revision D.3: Frisch, M. J.; Trucks, G. W.; Schlegel, H. B.; Gill, P. M. W.; Johnson, B. G.; Robb, M. A.; Cheeseman, J. R.; Keith, T.; Petersson, G. A.; Montgomery, J. A.; Raghavachari, K.; Al-Laham, M. A.; Zakrzewski, V. G.; Ortiz, J. V.; Foresman, J. B.; Cioslowski, J.; Stefanov, B. B.; Nanayakkara, A.; Challacombe, M.; Peng, C. Y.; Ayala, P. Y.; Chen, W.; Wong, M. W.; Andres, J. L.; Replogle, E. S.; Gomperts, R.; Martin, R. L.; Fox, D. J.; Binkley, J. S.; Defrees, D. J.; Baker, J.; Stewart, J. P.; Head-Gordon, M.; Gonzalez, C.; Pople, J. A.; Gaussian, Inc.: Pittsburgh, PA, 1995.
(33) Becke, A. *Phys. Rev. A* **1988**, *38*, 3098.
(34) Lee, C.; Yang, W.; Parr, R. G. *Phys. Rev. B* **1988**, *37*, 785.
(35) Perdew, J. P. *Phys. Rev. B* **1986**, *33*, 8822.
(36) Becke, A. D. *J. Chem. Phys.* **1993**, *98*, 5648.
(37) Perdew, J. P.; Wang, Y. *Phys. Rev. B* **1992**, *45*, 13244.
(38) CDA 2.1 Dapprich, S.; Frenking, G. Marburg 1995. Internet: ftp.chemie.uni-marburg.de, login: anonymous, directory: pub/cda.
(39) GAUSSIAN 92/DFT, Revision F.2: Frisch, M. J.; Trucks, G. W.; Schlegel, H. B.; Gill, P. M. W.; Johnson, B. G.; Wong, M. W.; Foresman, J. B.; Robb, M. A.; Head-Gordon, M.; Replogle, E. S.; Gomperts, R.; Andres, J. L.; Raghavachari, K.; Binkley, J. S.; Gonzalez, C.; Martin, R. L.; Fox, D. J.; Defrees, D. J.; Baker, J.; Stewart, J. J. P.; Pople, J. A.; Gaussian, Inc.: Pittsburgh, PA, 1993.
(40) Radius, U.; Bickelhaupt, F. M.; Ehlers, A. W.; Goldberg, N.; Hoffmann, R. *Inorg. Chem.* **1998**, *37*, 1080.
(41) Beagley, B.; Schmidling, D. G. *J. Mol. Struct.* **1974**, *22*, 466.
(42) Braga, D.; Grepioni, F.; Orpen, A. G. *Organometallics* **1993**, *12*, 1481.
(43) Huang, J.; Hedberg, K.; Davis, H. B.; Pomeroy, R. K. *Inorg. Chem.* **1990**, *29*, 3923.
(44) Huang, J.; Hedberg, K.; Pomeroy, R. K. *Organometallics* **1988**, *7*, 2049.

Table 1. Geometric Parameters[a] of $M(CO)_5$ (D_{3h})

method	$M-C_{ax}$	$M-C_{eq}$	$(C-O)_{ax}$	$(C-O)_{eq}$
		$Fe(CO)_5$		
BLYP[b]	1.837	1.834	1.159	1.162
BP86/Ziegler[c]	1.817	1.813	1.153	1.156
VWN/Delley[d]	1.776	1.774	1.145	1.147
BVWN/Delley[d]	1.846	1.851	1.154	1.159
BLYP/Delley[d]	1.837	1.834	1.156	1.158
BP86/Delley[d]	1.817	1.814	1.150	1.155
MP2/Frenking[e]	1.688	1.766	1.176	1.166
MCPF/Bauschlicher[f]	1.878	1.847	1.168	1.177
expt (gas phase[g])	1.807	1.827	1.152	1.152
expt (crystal[h])	1.811	1.803	1.117	1.133
		$Ru(CO)_5$		
BLYP[b]	1.994	2.010	1.157	1.162
B3LYP[b]	1.986	2.001	1.144	1.149
BP86/Ziegler[c]	1.968	1.960	1.150	1.157
VWN/Delley[d]	1.945	1.946		
BVWN/Delley[d]	2.013	2.025		
BLYP/Delley[d]	2.001	2.010		
MP2/Frenking[e]	1.943	1.952	1.162	1.165
expt (gas phase[i])	1.941	1.961	1.126	1.127
		$Os(CO)_5$		
BLYP[b]	1.992	1.983	1.159	1.165
B3LYP[b]	2.010	1.989	1.115	1.122
BP86/Ziegler[c]	2.000	1.975	1.147	1.156
MP2/Frenking[e]	1.963	1.945	1.163	1.168
expt (gas phase[j])	1.982	1.937	1.130	1.131

[a] All distances in Å. [b] Results from the present study. [c] Values taken from the nonlocal DFT study of Ziegler et al.[45] [d] Values taken from the DFT study of Delley et al.[46] [e] Values taken from the MP2 study of Ehlers and Frenking.[47] [f] Values taken from the correlated *ab initio* study of Bauschlicher and co-workers.[48] [g] Experimental gas-phase diffraction values.[41] [h] Experimental crystal structure values.[42] [i] Experimental gas-phase diffraction values.[43] [j] Experimental gas-phase diffraction values.[44]

Both DFT methods correctly predict the experimentally observed trend of the M−C distances (axial vs equatorial) for $Ru(CO)_5$, $Ru-C_{ax} < Ru-C_{eq}$, and $Os(CO)_5$, $Os-C_{ax} > Os-C_{eq}$, although the magnitude of the differences is smaller than that observed experimentally. In the case of $Fe(CO)_5$, the BLYP/BS1 calculations predict the $Fe-C_{ax}$ bond to be slightly longer than the $Fe-C_{eq}$ bond, by only 0.003 Å, in agreement with the trend from the experimental crystal structure,[41] but in disagreement with the trend found from the experimental gas-phase diffraction data.[42] In all of the $M(CO)_5$ complexes, the C−O distances of the axial and equatorial ligands are nearly equal, in both the calculations and experiment.

Availability of several previous computational studies of the metal pentacarbonyls of the Fe triad allows for a comparison of the accuracy of the geometries predicted by the DFT methods with a variety of correlated wave function methods. It should be noted that a direct comparison of the different methods is not entirely valid, since different basis sets were used in the various calculations. The previous nonlocal DFT calculations, in particular the BP86 calculations of Ziegler and co-workers[45] and the BLYP and BP86 calculations of Delley et al.,[46] predicted geometries which are quite close to those from the present work. In the case of $Fe(CO)_5$, the VWN local DFT results show very poor agreement with the experiment; surprisingly, the agreement is quite remarkable for $Ru(CO)_5$. The geometries obtained by Frenking et al.[47] with the MP2 method show very poor agreement for the first-row complex, but the agreement improves and matches the accuracy of our DFT calculations for the heavier congeners. Overall, the present BLYP/BS1 and B3LYP/BS1 geometries show better agreement with experiment than the MP2 calculations of Frenking, perhaps reflecting basis set effects.

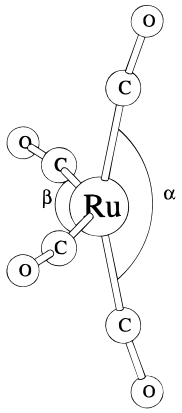

Figure 1. Structure of $Ru(CO)_4$.

2. $M(CO)_4$. The unsaturated $M(CO)_4$ product complexes may be formed via loss of a CO ligand from either the axial or equatorial position in the parent pentacarbonyl. Poliakoff et al.,[49,50] in low-temperature matrix-isolation IR studies, have shown that in the case of Fe, the dissociation of CO proceeds via loss of an equatorial CO, leading to a distorted T_d-like structure of C_{2v} symmetry. Although there has been some controversy surrounding the ground electronic state of $Fe(CO)_4$, the temperature-dependent magnetic circular dichroism experiments of Poliakoff and co-workers[51] have conclusively shown it to be paramagnetic. These findings have been supported by a number of theoretical studies,[45,46,48,52] all of which predict $Fe(CO)_4$ to have a $^3B_2$ ground electronic state, and a distorted C_{2v} T_d-like structure. Bogdan and Weitz,[53] in transient infrared spectroscopy kinetics studies, have concluded that the unsaturated CO dissociation products of the Ru and Os analogues have singlet ground states. These findings are fully supported by the theoretical study of Ziegler and co-workers.[45]

The present BLYP/BS1 calculations of the unsaturated $M(CO)_4$ carbonyl dissociation products are in full agreement with the previous findings of a preference for the dissociation of a CO ligand from the equatorial position. Our calculations predict $Fe(CO)_4$ to have a $^3B_2$ ground electronic state, while $Ru(CO)_4$ and $Os(CO)_4$ are predicted to have $^1A_1$ ground states. The lowest energy geometric conformer of each $M(CO)_4$ complex is predicted to have a distorted T_d-like C_{2v} structure, corresponding to the product formed by the removal of an equatorial CO from the parent pentacarbonyl. As expected, in forming the $M(CO)_4$ complex the $C_{ax}-M-C_{ax}$ angle, denoted hereafter as α, compresses while the $C_{eq}-M-C_{eq}$ angle, denoted β, expands toward the vacant site. This characteristic structure is illustrated in Figure 1 for the Ru analogue, while the values of the geometric parameters for all three $M(CO)_4$ complexes are collected in Table 2, along with the results of previous theoretical studies. It should be noted that all three of the lowest-energy $M(CO)_4$ conformers in their respective lowest-energy electronic states correspond to minima on their respective

(45) Li, J.; Schreckenbach, G.; Ziegler, T. *J. Am. Chem. Soc.* **1995**, *117*, 486.
(46) Delley, B.; Wrinn, M.; Lüthi, H. P. *J. Chem. Phys.* **1994**, *100*, 5785.
(47) Ehlers, A. W.; Frenking, G. *Organometallics* **1995**, *14*, 423.
(48) Barnes, L. A.; Rosi, M.; Baushlicher, C. W., Jr. *J. Chem. Phys.* **1991**, *94*, 2031.
(49) Poliakoff, M.; Turner, J. J. *J. Chem. Soc., Dalton Trans.* **1974**, 2276.
(50) Poliakoff, M.; Weitz, E. *Acc. Chem. Res.* **1987**, *20*, 408.
(51) Barton, T. J.; Grinter, R.; Thomson, A. J.; Davies, B.; Poliakoff, M. *J. Chem. Soc., Chem. Commun.* **1977**, 841.
(52) Daniel, C.; Benard, M.; Dedieu, A.; Wiest, R.; Veillard, A. *J. Phys. Chem.* **1984**, *88*, 4805.
(53) (a) Bogdan, P. L.; Weitz, E. *J. Am. Chem. Soc.* **1989**, *111*, 3163. (b) Bogdan, P. L.; Weitz, E. *J. Am. Chem. Soc.* **1990**, *112*, 639.

Table 2. Optimized Geometric Parameters[a] of $M(CO)_4$ (C_{2v})[b]

method	$M-C_{ax}$	$M-C_{eq}$	$(C-O)_{ax}$	$(C-O)_{eq}$	α[c]	β[d]
			$Fe(CO)_4$ ($^3B_2$)			
BLYP[e]	1.881	1.852	1.161	1.163	146	98
BP86/Ziegler[f]	1.859	1.820	1.156	1.160	147.4	99.4
MCPF/Bauschlicher[g]	1.879	1.885	1.169	1.175	150	104
			$Fe(CO)_4$ ($^1A_1$)			
BLYP[e]	1.824	1.814	1.164	1.166	145	137
BP86/Ziegler[f]	1.834	1.793	1.153	1.160	167.7	129.8
MCPF/Bauschlicher[g]	1.910	1.875	1.181	1.178	151	125
MP2/Frenking[h]	1.726	1.713	1.170	1.178	170.0	135.9
			$Ru(CO)_4$ ($^1A_1$)			
BLYP[e]	1.987	1.971	1.160	1.164	158	143
B3LYP[e]	1.986	1.965	1.145	1.150	169	144
BP86/Ziegler[f]	1.991	1.991	1.149	1.153	167.4	144.0
MP2/Frenking[h]	1.951	1.904	1.161	1.171	179.4	137.4
			$Os(CO)_4$ ($^1A_1$)			
BLYP[e]	1.958	1.959	1.166	1.165	146	146
BP86/Ziegler[f]	2.059	2.040	1.149	1.151	161.0	152.0
MP2/Frenking[h]	1.942	1.909	1.165	1.172	157.0	138.9

[a] Bond lengths in Å and angles in deg. [b] Structures correspond to that formed by loss of an equatorial CO from $M(CO)_5$. [c] The $C_{ax}-M-C_{ax}$ angle. [d] The $C_{eq}-M-C_{eq}$ angle. [e] Results from the present study. [f] Values taken from the nonlocal DFT study of Ziegler et al.[45] [g] Values taken from the correlated *ab initio* study of Bauschlicher et al.[48] [h] Values taken from the MP2 study of Frenking *et al.*[47]

potential energy surfaces, as confirmed by harmonic vibrational analysis. This supports the dissociative rate determining step proposed in the kinetics study.[54,55] The corresponding $^1A_1$ $Fe(CO)_4$, $^3B_2$ $Ru(CO)_4$, and $^3B_2$ $Os(CO)_4$ excited states (in the C_{2v} symmetry) are predicted to lie 4−18 kcal/mol above their respective ground states. The $M(CO)_4$ geometric conformers of C_3 symmetry, in which an axial CO has been removed, were found to lie even higher in energy than the C_{2v} excited states. For example, in $Fe(CO)_4$ the singlet and triplet states of the C_3 conformers were 10 and 25 kcal/mol higher in energy than the $^1A_1$ excited state of the C_{2v} conformer.

In general, the BLYP/BS1 geometries of the $M(CO)_4$ complexes are very similar to those found in previous theoretical studies, as illustrated in Table 2. Perhaps the largest exception to this generalization are Frenking's[47] MP2-optimized parameters for the $^1A_1$ excited state of $Fe(CO)_4$, and the $C_{ax}-M-C_{ax}$ (α) and $C_{eq}-M-C_{eq}$ (β) angles in the $^1A_1$ ground state of $Ru(CO)_4$. Our BLYP/BS1 $M(CO)_4$ geometries appear to be slightly more distorted from their respective parent pentacarbonyls than found in the previous ab initio or DFT calculations.

The present BLYP/BS1 calculations, as well as the previous theoretical calculations, predict significant differences in the geometries of the triplet and singlet electronic states of $Fe(CO)_4$. The C−O distances and α angles ($C_{ax}-M-C_{ax}$) are equivalent in the two states. However, the M−C distances are slightly shorter in the $^1A_1$ excited state than in the $^3B_2$ ground state and there is a significant difference between the values of the β angle ($C_{eq}-M-C_{eq}$) in the two states. It should be noted that Poliakoff et al.[49] have estimated values of 145° and 120° for the α and β angles, based on their matrix isolation IR spectroscopy measurements. All of the computational results shown in Table 2 underestimate Poliakoff's value of the β angle.

Comparison of the BLYP/BS1 optimized geometries of the three $^1A_1$ $M(CO)_4$ complexes reveals that the spin-allowed dissociation of an equatorial CO ligand results in a larger compression of the axial ligands toward the vacant site in the Fe and Os complexes than in the Ru complex. Interestingly, the same trend is not observed for the expansion of the $C_{eq}-M-C_{eq}$ (β) angle toward the vacant site, for which Os > Ru > Fe. For each of the metals of the triad, the spin-allowed dissociation process leads to a shortening of both of the M−C distances. However, the spin-forbidden CO dissociation leading to $Fe(CO)_4$ in the $^3B_2$ state results in a lengthening of both of the M−C distances. On the basis of the predicted geometric changes of the triplet and singlet states of $Fe(CO)_4$ it would appear that the spin-allowed and spin-forbidden CO dissociations proceed along quite different reaction pathways.

As seen previously in the $M(CO)_5$ complexes, the $^1A_1$ $Ru(CO)_4$ geometry optimized with the B3LYP functional yielded shorter C−O distances, with very little change in the M−C distances relative to the BLYP optimized geometries. At the B3LYP/BS1 level the $C_{ax}-M-C_{ax}$ (α) angle is predicted to be less compressed than in the BLYP/BS1 structure.

Table 3. Selected Geometric Parameters[a] of $M(CO)_4(C_2H_2)$ (C_{2v})

	$Fe(CO)_4(C_2H_2)$	$Ru(CO)_4(C_2H_2)$		$Os(CO)_4(C_2H_2)$		
parameter	BLYP	BLYP	expt[b]	BLYP	B3LYP	expt[b]
$M-C_{ax}$	1.843	1.993	1.967	1.989	1.981	1.972
$M-C_{eq}$	1.823	2.001	1.966	1.972	1.963	1.969
$M-C_{ac}$	2.140	2.264	2.125	2.247	2.220	2.142
$(C-C)_{ac}$	1.265	1.271	1.276	1.283	1.276	1.276
$(C-O)_{ax}$	1.159	1.158	1.130	1.159	1.145	1.128
$(C-O)_{eq}$	1.164	1.162	1.129	1.165	1.152	1.115
$C_{ax}-M-C_{ax}$	173.5	172.7	172.7	171.7	171.1	172.6
$C_{eq}-M-C_{eq}$	110.1	107.0	98.7	104.7	104.3	95.2
$C_{ac}-M-C_{ac}$	34.4	32.6	35.0	33.2	33.4	34.7
$C_{ax}-M-C_{eq}$	91.9	92.2	93.5	92.5	92.7	92.8
$C_{ax}-M-C_{ac}$	86.9	86.5	86.5	86.0	85.8	86.5
$C_{eq}-M-C_{ac}$	107.8	110.2	113.2	111.1	111.2	115.1

[a] Bond lengths in Å and angles in deg. [b] Values correspond to the crystal structures of the related $Ru(CO)_4[C_2(CF_3)_2]$ and $Os(CO)_4[C_2(CF_3)_2]$ species.[9]

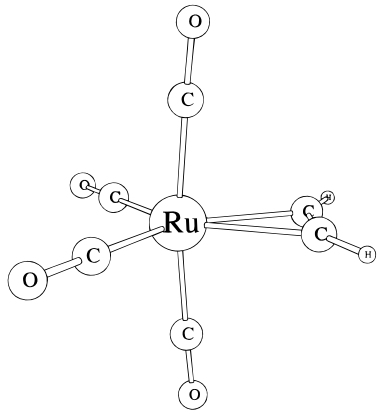

Figure 2. Structure of $Ru(CO)_4(C_2H_2)$.

B. Structures of the Alkyne Complexes. 1. $M(CO)_4(C_2H_2)$. The geometries of the saturated alkyne-substituted complexes, $M(CO)_4(C_2H_2)$, were optimized under C_{2v} symmetry, using the BLYP/BS1 approach. The results are summarized in Table 3, and the structure of the Ru compound is shown in Figure 2. Geometric parameters optimized with the B3LYP method are also presented in Table 3, together with experimental parameters from the crystal structures of the related alkyne complexes $Ru(CO)_4[C_2(CF_3)_2]$ and $Os(CO)_4[C_2(CF_3)_2]$.[9]

The BLYP/BS1 method predicts the following trend for the M−C distances: Fe−C < Os−C < Ru−C. Iron, with the smallest covalent radius, would be expected to have the smallest M−C bond lengths. However, as the covalent radii of Ru and Os are approximately equal, the shorter Os−C bond may be an

(54) Huq, R. A.; Poe, A. J.; Chawla, S. *Inorg. Chim. Acta* **1980**, *38*, 121.

(55) Shen, J.-K.; Gao, Y.-C.; Shi, Q.-Z.; Basolo, F. *Inorg. Chem.* **1989**, *28*, 4304.

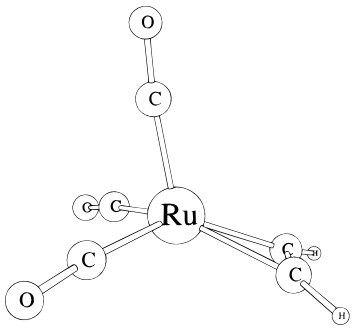

Figure 3. Structure of $Ru(CO)_3(C_2H_2)$.

indication of stronger bonding between the metal and the CO and C_2H_2 ligands for Os than for Ru. The C−C distances of the bound acetylene ligand increase down the triad, and are substantially longer than in free acetylene, 1.202 Å.[56] As expected, coordination of acetylene to the metal has decreased the C−C bond order, and rehybridized the acetylenic carbons toward ethylenic sp^2 carbons, as illustrated in Figure 2. There are no significant differences among the C−O bond lengths or the bond angles for the metals of the triad.

The agreement between the BLYP/BS1 geometries and the experimental crystal structures of the Ru and Os hexafluorobut-2-yne complexes is good considering the significant differences between our model alkyne and the experimental one. In both the Ru and Os analogues the BLYP/BS1 calculations predict longer M−C and C−O distances than observed experimentally. The only bond angle that is markedly different from its experimental value is the $C_{eq}-M-C_{eq}$ angle, perhaps due to the different steric and electronic demands of the model alkyne ligand and those of the actual complex. Again the overall agreement with experiment appears to be slightly better with the B3LYP functional than with the BLYP functional.

2. $M(CO)_3(C_2H_2)$. As in the metal pentacarbonyls, CO dissociation may occur from either an axial or equatorial position in the parent $M(CO)_4(C_2H_2)$ complex. The axial CO dissociation products, optimized under C_s symmetry constraints, were found to be more stable by 10-20 kcal/mol than the equatorial CO dissociation products. Harmonic vibrational analysis characterized all of the $M(CO)_3(C_2H_2)$ axial CO dissociation products as stable intermediates. This agrees with the experimental kinetics study of Takats and Jordan,[7] which showed that the rate determining step for the CO substitution reactions in the $M(CO)_4[C_2(CF_3)_2]$ complexes was the dissociative loss of CO. Loss of an axial carbonyl ligand results in the acetylene ligand bending downward out of plane toward the vacant axial site. The lone axial CO ligand bends back away from the alkyne, resulting in a distorted square-pyramidal type structure, as illustrated in Figure 3 for the Ru congener. The BLYP/BS1 structural parameters are summarized in Table 4, along with the B3LYP/BS1 values. Although there are no experimental structural data for these particular unsaturated alkyne tricarbonyl complexes, the crystal structures of the related $Fe(CO)_2(P(C_6H_{11})_3)[\eta^2-C_2(CF_3)_2]$ and $Os(CO)(P(^iPr)_3)_2[\eta^2-C_2Ph_2]$ complexes exhibit a similar distorted square-pyramidal geometry and their relevant structural parameters are given in Table 4.[57,58] The deviation between the experimental and calculated M−C distances is less than 0.05 Å, while that for the C−C distance of the alkyne ligand is less than 0.02 Å. The differences between our model complex and the experimental ones are too large to warrant any direct comparison of most of the angles. However, the computed $C_{ac}-M-C_{ac}$ angle is within 1° of that found experimentally for both complexes. Not surprisingly, the largest differences are for the bend-back angle of the alkyne ligand, computed to be much smaller for acetylene than found experimentally, reflecting the varying steric, electronic, and environmental effects of the different alkynes.

Table 4. Selected Geometric Parameters[a] of $M(CO)_3(C_2H_2)$ (C_s)

	$Fe(CO)_3(C_2H_2)$		$Ru(CO)_3(C_2H_2)$	$Os(CO)_3(C_2H_2)$		
parameter	BLYP	expt[b]	BLYP	BLYP	B3LYP	expt[c]
$M-C_{ax}$	1.778		1.900	1.905	1.896	
$M-C_{eq}$	1.824	1.769	1.989	1.965	1.957	1.817
$M-C_{ac}$	1.904	1.868	2.072	2.050	2.031	2.035
$(C-C)_{ac}$	1.316	1.294	1.317	1.335	1.329	1.318
$(C-O)_{ax}$	1.166		1.168	1.170	1.156	
$(C-O)_{eq}$	1.164	1.149	1.163	1.166	1.152	1.181
$C_{eq}-M-C_{eq}$	107.4	103.3	105.7	102.8	102.5	
$C_{ac}-M-C_{ac}$	40.4	40.5	37.1	38.0	38.2	37.8
$C_{ax}-M-C_{eq}$	93.3	90.9	90.7	90.9	90.5	
$C_{ax}-M-C_{ac}$	117.6		121.4	122.8	122.2	
$C_{eq}-M-C_{ac}$	100.1	102.9	102.6	102.8	103.2	

[a] Bond lengths in Å and angles in deg. [b] Values taken from the crystal structure of $Fe(CO)_2(P(C_6H_{11})_3)[\eta^2-C_2(CF_3)_2]$.[57] The phosphine occupies the axial position. The value for the $C_{ax}-M-C_{eq}$ angle actually corresponds to the $P-M-C_{eq}$ angle. [c] Values taken from the crytsal structure of $Os(CO)(P(^iPr)_3)_2[\eta^2-C_2Ph_2]$.[58] The lone CO ligand occupies an equatorial position.

A comparison of the optimized geometries of the unsaturated $M(CO)_3(C_2H_2)$ complexes with those of their parent molecules reveals the structural changes that occur upon dissociation of the axial carbonyl: contraction of the remaining $M-C_{ax}$ bond and of the $M-C_{ac}$ bonds, coupled with an elongation of the C−C bond of the acetylene ligand. There is little change in the $M-C_{eq}$ and C−O bond lengths upon CO loss. Hence, based on these structural changes it would appear that dissociation of the axial CO from the alkyne complexes increases the amount of bonding between the acetylene ligand and the metal, coupled with a decrease in the C−C bond order of the acetylene ligand. The structural data support the rationalization, proposed by Takats and Jordan,[7] for the increased CO lability of the alkyne complexes due to stabilization of the unsaturated transition state via an increased donation from the alkyne to the metal. Furthermore, the structural changes are consistent with an increased bonding character between the metal and the remaining axial CO. When compared to the BLYP optimized structures, the B3LYP functional predicts changes in the geometry of the unsaturated $M(CO)_3(C_2H_2)$ compound similar to those discussed above for the saturated alkyne complexes.

C. Carbonyl Bond Dissociation Energies. The first carbonyl bond dissociation energies (CO BDE) of the d^8 $M(CO)_5$ and $M(CO)_4(C_2H_2)$ species (where M = Fe, Ru, and Os) are summarized in Table 5, along with the results of previous theoretical and experimental studies. The CO BDEs were calculated from the difference in total energies of the parent complex and the dissociation products at their respective optimized geometries. The BLYP/BS1 optimized geometries were used throughout. The validity of using the BLYP/BS1 geometries as representative geometries for the other functionals was tested by optimizing the reactant and CO dissociation product of $Ru(CO)_5$ and $Os(CO)_4(C_2H_2)$ with the B3LYP functional. As seen in Table 5, the B3LYP/BS1//B3LYP/BS1 CO BDE values for $Ru(CO)_5$ and $Os(CO)_4(C_2H_2)$ are 25.0 and 15.2 kcal/mol, respectively, and they are essentially identical to the values obtained with the BLYP/BS1 geometries (B3LYP/BS1//BLYP/BS1), 25.2 and 15.0 kcal/mol. Hence, we believe

(56) Kostyk, E.; Welsh, H. L. *Can. J. Phys.* **1980**, *58*, 912.
(57) Cooke, J.; McDonald, R. Personal communication.
(58) Espuelas, J.; Esteruelas, M. A.; Lahoz, F. J.; Lopez, A. M.; Oro, L. A.; Valero, C. *J. Organomet. Chem.* **1994**, *468*, 223.

Table 5. First Carbonyl Bond Dissociation Energies (kcal/mol) of $M(CO)_5$ and $M(CO)_4(C_2H_2)$

	$M(CO)_5$				$M(CO)_4(C_2H_2)$			
	Fe				Fe			
method	S[a]	T[b]	Ru	Os	S[c]	T[d]	Ru	Os
BLYP[e]	37.3	33.6	24.2	28.7	12.1	30.7	18.0	14.5
	(34.5)	(30.3)	(22.4)	(26.9)	(10.5)		(16.5)	(13.1)
BP86[f]	46.1	42.6	31.6	37.0	17.8		22.6	19.7
B3LYP[f]	38.2	26.6	25.2	32.3	11.3		19.1	15.0
			(25.0)					(15.2)
B3PW91[f]	44.2	31.7	30.0	38.0	14.8		21.7	18.4
RHF				27.9			10.2	6.0
BP86/Ziegler[g]	45.7	43.9	33.0	34.7				
VWN/Delley[h]	64	71						
BVWN/Delley[h]	30	32						
BLYP/Delley[h]	38	41						
CISD/Veillard[i]		35.7						
		(42.8)						
CCSD(T)/Frenking[j]	46.5		30.9	42.4				
MCPF/Bauschlicher[k]	39	23.9						
expt	41.5[l]	55[m]	27.6[n]	31.9[o] (30.6)[p]	21.0[q]		25.0[q]	23.8[q]
	± 3	± 11	± 0.4	± 0.6 (± 0.3)	± 0.5		± 0.6	± 0.2

[a] Value corresponds to the dissociation pathway leading to $^1A_1$ $Fe(CO)_4$ (loss of an equatorial CO). [b] Value corresponds to the dissociation pathway leading to $^3B_2$ $Fe(CO)_4$ (loss of an equatorial CO). [c] Value corresponds to the dissociation pathway leading to $^1A'$ $Fe(CO)_3(C_2H_2)$ (loss of an axial CO). [d] Value corresponds to the dissociation pathway leading to $^3A'$ of $FeCO_3(C_2H_2)$ (loss of an equatorial CO). [e] The values in parentheses include zero-point energy corrections. [f] Values obtained from single point energy calculations with use of the specified functional at the respective BLYP optimized geometries (i.e. BP86 denotes results from BP86/BS1//BLYP/BS1). [g] Values taken from the nonlocal DFT calculations of Ziegler et al.[45] [h] Values taken from the DFT study of Delley et al.[46] [i] Values taken from the CISD study of Veillard et al.[52] The second value includes the Davidson correction. [j] Values taken from the CCSD(T) calculations of Ehlers and Frenking.[47] [k] Values taken from the Modified Coupled Pair Functional (MCPF) calculations of Bauschlicher and co-workers.[48] [l] Value determined from a pulsed laser pyrolysis study in the gas phase by Lewis et al.[59] [m] Value determined from a laser photoelectron spectroscopy study in the gas phase by Engelking and Lineberger.[60] [n] Value corresponds to $\Delta H^{\ddagger}$ from the solution kinetics study of Huq et al.[54] [o] Value corresponds to $\Delta H^{\ddagger}$ from the solution kinetics study of Pearson et al.[7] [p] Value corresponds to $\Delta H^{\ddagger}$ from the solution kinetics study of Basolo and co-workers.[55] [q] Value corresponds to $\Delta H^{\ddagger}$ from the kinetics study of the related species $M(CO)_4[C_2(CF_3)_2]$.[7] Recent solution kinetics experiments have found a $\Delta H^{\ddagger}$ value of 21.8 ± 0.2 kcal/mol for $Os(CO)_4(C_2H_2)$.[8]

that the errors introduced by not re-optimizing the geometries with each functional tend to cancel out when the CO BDE is computed.

All of our DFT calculations correctly predict a reduction in the first CO BDE values of the alkyne-substituted species relative to their respective parent carbonyl complex, by about 6−20 kcal/mol depending on the method and the metal. All of the DFT methods also predict the reduction in the CO BDE of the Ru alkynes to be the smallest among the metals of the triad (about 6−9 kcal/mol) while that for the Fe and Os alkynes is significantly larger (about 15−20 kcal/mol). These results are in accord with the kinetics studies which showed that the alkyne complexes had smaller $\Delta H^{\ddagger}$ values than the corresponding pentacarbonyls and that the increase in reactivity of the alkynes was spectacular for Fe, good for Os, and modest for Ru.[7]

As illustrated in Table 5, the different DFT functionals predict a wide range of CO BDE values, especially for the pentacarbonyls. It should be noted that a direct comparison of the calculated values to the experimental ones is not entirely valid for all the systems studied. For instance, the experimental values listed in Table 5 for the Ru and Os analogues of both the alkyne and carbonyl complexes were taken from solution kinetics study, and they correspond to $\Delta H^{\ddagger}$ values and not to CO BDEs. Although the experimental CO BDE value for the dissociation to singlet $Fe(CO)_4$ from the gas-phase laser pyrolysis study of Lewis et al.[59] appears to be quite reasonable, the corresponding value for dissociation to the triplet state, as measured by gas-phase laser photoelectron spectroscopy by Engelking and Lineberger,[60] is certainly questionable. Not only is there a huge error associated with it, 11 kcal/mol (20% of the value), but this value implies that the triplet state is less stable than the singlet state, in contrast to the earlier findings of a triplet ground state of Poliakoff and co-workers.[51] It is likely that these experiments were probing an excited triplet state, rather than the ground electronic state.

The dependence of the calculated CO BDE values on the metal atom is shown in Figure 4 for both the pentacarbonyls and the alkyne complexes, along with the respective experimental trends. From Figure 4, one can see that the experimental CO BDE/$\Delta H^{\ddagger}$ trends among the $M(CO)_5$ species, Fe > Os > Ru, and the $M(CO)_4(C_2R_2)$ species, Ru > Os > Fe, are faithfully reproduced by all of our nonlocal DFT calculations. A comparison of the CO BDEs computed from the different functionals shows several interesting features. It would appear that on the basis of the metal dependence of the CO BDE values of the $M(CO)_5$ compounds, we can group the four different functionals used into two sets. The metal dependences predicted by the BLYP and BP86 functionals mirror one another, and therefore form one set, while the B3LYP and B3PW91 form the other. On the other hand, the CO BDEs predicted by the BLYP/BS1//BLYP/BS1 and B3LYP/BS1//BLYP/BS1 calculations, for both the pentacarbonyls and alkyne complexes, are always smaller in magnitude than those predicted by the BP86/BS1//BLYP/BS1 and B3PW91/BS1//BLYP/BS1 methods. Hence, it would appear that the exchange functional, Becke vs Becke3, is crucial in determining the magnitude of the differences between the CO BDEs of the different metals, while the correlation functional affects the magnitudes of each individual CO BDE.

The compilation of CO BDE values in Table 5 allows for a comparison of a variety of different DFT and correlated wave function theory methods. However, since different basis sets were used in these studies, the differing values reflect more than

(59) Lewis, K. E.; Golden, D. M.; Smith, G. P. *J. Am. Chem. Soc.* **1984**, *106*, 3905.

(60) Engelking, P. C.; Lineberger, W. C. *J. Am. Chem. Soc.* **1979**, *101*, 5569.

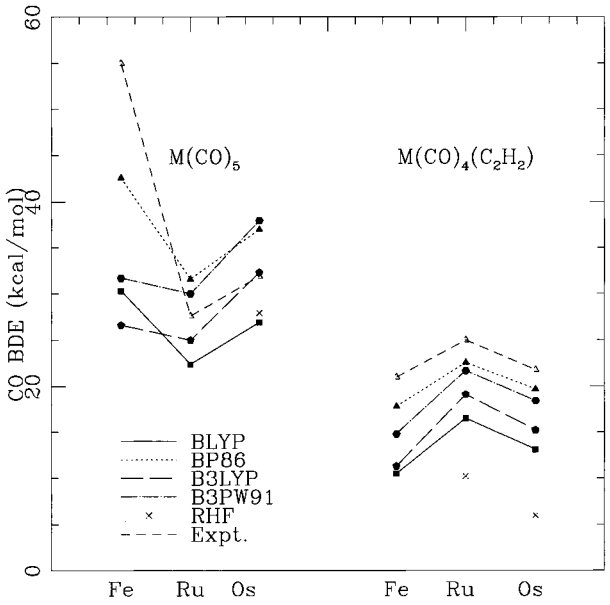

Figure 4. First CO bond dissociation energies of $M(CO)_5$ and $M(CO)_4(C_2H_2)$. The values correspond to dissociation leading to the most stable products. The filled squares correspond to the BLYP/BS1//BLYP/BS1 values, the filled triangles correspond to the BP86/BS1//BLYP/BS1 values, the filled pentagons correspond to the B3LYP/BS1//BLYP/BS1 values, the filled hexagons correspond to the B3PW91/BS1//BLYP/BS1 values, and the crosses correspond to the RHF/BS1//RHF/BS1 values. The experimental values are represented by the open triangle symbols.

mere differences in the methods themselves. Ziegler's BP86-DFT results[45] show, not surprisingly, good agreement with our BP86 values. The CCSD(T)//MP2 computed values of Frenking et al.[47] are larger than our BLYP and B3LYP values, but are in accord with our BP86 and B3PW91 values. Veillard et al.[52] predict a value of 35.7 kcal/mol for the CO BDE of $Fe(CO)_5$ to the triplet state at the CISD level of theory, while Bauschlicher and co-workers[48] estimate it to be 23.9 kcal/mol, the lowest estimate. As discussed previously, $Fe(CO)_4$ is known to possess a triplet electronic ground state with a fairly low-lying excited singlet state; the singlet−triplet energy gaps for $Fe(CO)_4$ are summarized in Table 6. The BLYP and BP86 functionals predict a singlet−triplet splitting of the same magnitude but smaller than that predicted by the B3LYP and B3PW91 functionals. This suggests that the Becke3 functional has a tendency to destabilize the excited singlet state more than Becke's original gradient-corrected functional. Interestingly, Delley et al.,[46] using a variety of local and nonlocal density functionals, incorrectly predict the singlet state to be lower in energy than the triplet state, by 2−7 kcal/mol. Bauschlicher et al.[48] predict a fairly large $Fe(CO)_4$ singlet−triplet splitting of 15.1 kcal/mol, slightly larger but of the same order of magnitude as that from the present B3LYP and B3PW91 calculations. In the case of $Ru(CO)_4$ and $Os(CO)_4$, the current BLYP calculations predict the singlet state to be lower than the triplet state by 16 and 18 kcal/mol, respectively. This is in agreement with the conclusions drawn by Bogdan and Weitz based on their transient IR spectroscopy studies.[53]

D. Reaction Profiles for CO Dissociation from $M(CO)_5$ and $M(CO)_4(C_2H_2)$. The differences between the present CO BDE values and the experimental $\Delta H^{\ddagger}$ values are much smaller for the metal pentacarbonyls than for the alkyne-substituted complexes. The energy profile along the reaction coordinate for carbonyl dissociation from the pentacarbonyls must therefore be quite flat with the top of the barrier being nearly equivalent to the energy of the dissociation products, while that of the alkyne complexes must possess a barrier that relaxes down to the products. To test this, the CO dissociation reaction trajectories were simulated for each of the $M(CO)_5$ complexes and the Ru analogue of the alkyne-substituted complex via constrained geometry optimizations of the complexes at fixed distances between the departing CO ligand and the metal. The departing CO ligand was forced to dissociate along the M−C bond, thereby constraining the optimizations to C_{2v} and C_s symmetry for the $M(CO)_5$ and $Ru(CO)_4(C_2H_2)$ species, respectively. In addition, all of the CO distances were fixed. Figure 5 displays the simulated CO dissociation trajectories along the spin-allowed singlet pathway for $Ru(CO)_5$ and $Os(CO)_5$. As expected, they are both flat, featureless trajectories with no apparent energy difference between the barrier maximum and the dissociation products. The difference in the total energies of the isolated products and the reaction trajectories for large values of the reaction coordinate may be attributed to the optimization and symmetry restrictions imposed. The maximum energy of the $Ru(CO)_5$ trajectory occurs when the departing CO is roughly 4.8 Å from the metal, while in $Os(CO)_5$ it occurs around 3.7 Å. Although this is a very rough estimate of the position of the transition state, the earlier transition state for $Os(CO)_5$ is in agreement with the conclusions drawn by Basolo and co-workers,[55] based on solution kinetics measurements. Initial characterization of these maximum energy points, via the energy Hessian, revealed four imaginary frequencies for the dissociating $Ru(CO)_5$ system, and three imaginary frequencies for the $Os(CO)_5$ system. In both cases, all the imaginary frequencies were smaller than 50 cm^{-1}. Due to the flat nature of the potential energy surfaces near the barrier maximum, no further attempt was made to locate the true transition state. However, it is this flatness of the reaction trajectories which validates a comparison of our computed CO BDEs to experimental $\Delta H^{\ddagger}$ values. The reaction trajectory for CO dissociation from $Fe(CO)_5$, shown in Figure 6, is more complicated due to the triplet ground electronic state of the unsaturated $Fe(CO)_4$ product complex. Hence, it was necessary to simulate not only the dissociation of CO from $Fe(CO)_5$ to singlet $Fe(CO)_4$, as done in the Ru and Os trajectories, but also the trajectory leading to $^3B_2$ $Fe(CO)_4$. This was accomplished by optimizing the geometry of the $^3B_2$ $Fe(CO)_4 + {}^1\Sigma^+$ CO system as the CO ligand was gradually brought closer and closer to the $^3B_2$ $Fe(CO)_4$ fragment. The reaction trajectory along the $^1A_1$ dissociation pathway is flat and featureless with no relaxation from the barrier to the products, as seen in the Ru and Os trajectories. The $^1A_1$ pathway is predicted to be the lowest-energy reaction trajectory until the dissociating CO ligand becomes separated from the metal by about 3.5−4.0 Å at which point the system would undergo a crossing to the $^3B_2$ state, and continue to the lowest energy dissociation products, $^3B_2$ $Fe(CO)_4$ and $^1\Sigma^+$ CO. The reaction trajectory for a high-lying $^3A_1$ excited state is also shown in Figure 6; however, it is most likely thermally inaccessible.

The simulated reaction trajectory for the dissociation of an axial carbonyl ligand from $Ru(CO)_4(C_2H_2)$ is displayed in Figure 7. Unlike the $M(CO)_5$ carbonyl dissociation trajectories, the energy profile for this trajectory increases to a maximum and then relaxes down to the products. The extent of this relaxation is quite modest, about 2−4 kcal/mol. The maximum occurs when the departing CO ligand is about 3.0−3.5 Å from the metal. An estimated 21 kcal/mol for $\Delta H^{\ddagger}$ may be obtained from the plot, quite close to the value of 25.0 kcal/mol obtained from kinetics measurements on the related Ru hexafluorobut-2-yne

Table 6. Singlet−Triplet Spacings[a] (kcal/mol) of $Fe(CO)_4$

	BLYP[b]	BP86[b]	B3LYP[b]	B3PW91[b]	BP86[c]	VWN[d]	BVWN[d]	BLYP[d]	MCPF[e]
ΔE(T−S)	−3.8	−3.4	−11.6	−12.5	−1.7	7	2	3	−15.1

[a] Computed as $\Delta E(T-S) = E(T) - E(S)$. If $\Delta E(T-S) < 0$, the triplet state is more stable, if $\Delta E(T-S) > 0$, the singlet state is more stable. [b] Values taken from the present study. The values of $\langle S^2 \rangle$ were in the range 2.02−2.05. [c] Value taken from the nonlocal DFT study of Ziegler et al.[45] [d] Value taken from the DFT study of Delley and co-workers.[46] [e] Value taken from the Modified Coupled Pair Functional (MCPF) calculations of Bauschlicher and co-workers.[48]

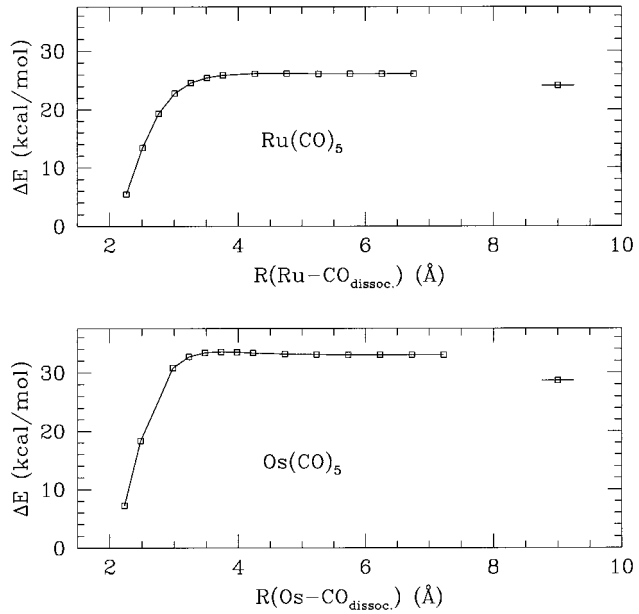

Figure 5. CO dissociation trajectories for $Ru(CO)_5$ and $Os(CO)_5$. The spin-allowed singlet pathways are shown. The energy is relative to that of the $M(CO)_5$ reactant complex. The reaction coordinate corresponds to the distance between the metal and the exiting CO ligand. The isolated point around 9 Å corresponds to the energy of the isolated dissociation products: $^1A_1$ $M(CO)_4$ + $^1\Sigma^+$ CO.

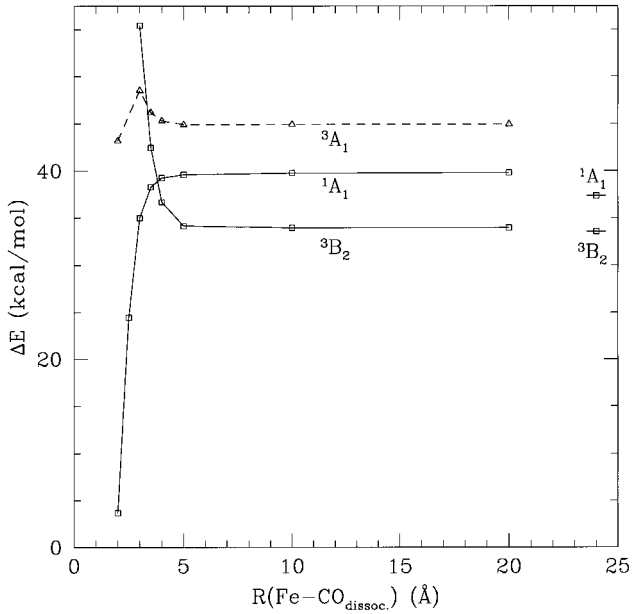

Figure 6. CO dissociation trajectories for $Fe(CO)_5$. The energy is relative to that of the $M(CO)_5$ reactant complex. The reaction coordinate corresponds to the distance between the metal and the exiting CO ligand. The isolated points around 9 Å correspond to the energy of the isolated dissociation products: $^1A_1$ $Fe(CO)_4$ + $^1\Sigma^+$ CO and $^3B_2$ $Fe(CO)_4$ + $^1\Sigma^+$ CO.

complex. The difference between the limiting value of the reaction trajectory and the energy of the isolated products can again be attributed to the symmetry and structural constraints imposed during optimization. Our calculations predict an earlier transition state and thus one of less bond-breaking character for the alkyne-substituted complex than for the pentacarbonyl, at least for the Ru species.

In summary, the computed CO dissociation reaction trajectories along the spin-allowed singlet pathways for all three of the $M(CO)_5$ complexes are predicted to be flat, with no apparent stabilization of the unsaturated $M(CO)_4$ dissociation product with respect to the transition state, while in $Ru(CO)_4(C_2H_2)$ the unsaturated dissociation product is predicted to be stabilized by a few kilocalories per mole with respect to the transition state. As alluded to by Takats and Jordan,[7] the alkyne ligand must be playing an active role in the stabilization of the unsaturated $M(CO)_3$(alkyne) intermediate. The origin of this stabilization is addressed in the following section.

E. The Role of the Acetylene Ligand. To probe the origin of the reduced CO BDE values of the alkyne complexes with respect to the parent pentacarbonyls, it was necessary to assess the role of the acetylene ligand in both the reactant complex, $M(CO)_4(C_2H_2)$, and the CO dissociated $M(CO)_3(C_2H_2)$ compound. Metal−olefin bonding is commonly described in terms of the well-known Dewar−Chatt−Duncanson model[61] of synergistic alkene → M σ bonding (i.e. donation from the occupied π orbital of the alkene to an empty metal orbital of proper σ symmetry) and M→alkene π back-donation (i.e. donation from an occupied metal orbital of π symmetry into the empty π^* alkene orbital). It is easy to extrapolate this model to the

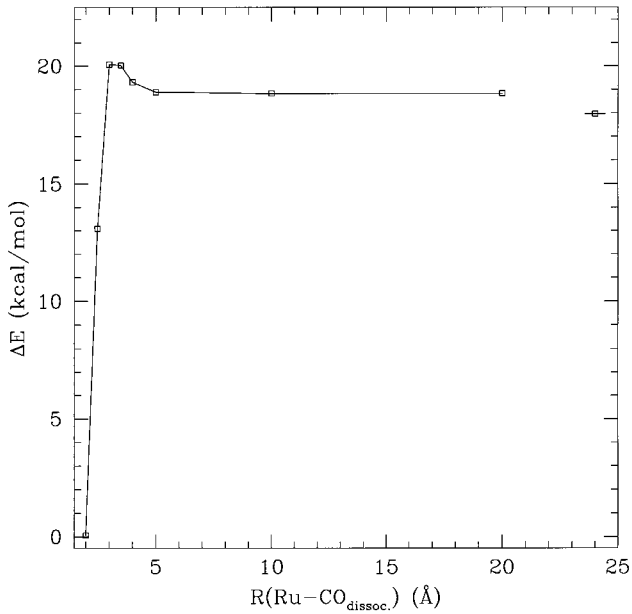

Figure 7. CO dissociation trajectory for $Ru(CO)_4(C_2H_2)$. The energy is relative to that of the $M(CO)_4(C_2H_2)$ reactant complex. The reaction coordinate corresponds to the distance between the metal and the exiting CO ligand. The isolated point around 24 Å corresponds to the energy of the isolated dissociation products: $^1A'$ $Ru(CO)_3(C_2H_2)$ + $^1\Sigma^+$ CO.

(61) Cotton, F. A.; Wilkinson, G. *Advanced Inorganic Chemistry*, 5th ed.: John Wiley and Sons: New York, 1988.

bonding between an alkyne and a metal, since the only difference is due to the presence of a second occupied π orbital that may donate to the metal, and a second π^* orbital available to accept electron density from the metal. In the formal electron-counting scheme alkynes may be treated as a two-electron donor when only one of the π orbitals is involved in bonding to the metal and as a four-electron donor when both of its π orbitals actively donate to the metal atom. The reactant complex, $M(CO)_4(C_2H_2)$, is a saturated 18-electron species, with the acetylene ligand contributing two electrons. Removal of a carbonyl leads to $M(CO)_3(C_2H_2)$, which is formally an unsaturated 16-electron complex, if acetylene remains a two-electron donor. On the other hand, counting acetylene as a four-electron donor gives the complex a saturated 18-electron count. It is this variable electron-donor ability of the acetylene that has been proposed by Takats and Jordan to account for the observed increased reactivity of the alkyne-substituted species with respect to the parent pentacarbonyl.[7] The alkyne may act as a four-electron donor to stabilize the otherwise unsaturated CO dissociation transition state/product, thereby leading to an increased reactivity, and a decreased CO BDE. This stabilization is not available in the pentacarbonyl, since the CO ligand does not have a second low-lying orbital to participate in donation to the metal. In the present work, the charge decomposition analysis (CDA) scheme of Frenking et al.[23] along with Bader's atoms-in-molecules (AIM) analysis of the electron density topology[24,25] were used to probe the stabilization of $M(CO)_3(C_2H_2)$.

1. CDA Results. Frenking's CDA scheme attempts to quantify donor−acceptor molecular interactions in terms of common Dewar−Chatt−Duncanson model concepts (i.e. donation, back-donation, and repulsion). CDA gives quantitative information regarding the change in the electronic structure of a complex, AB, due to the interactions between the two fragments A and B, based solely on orbital interactions. It is a linear combination of fragment orbitals-molecular orbital method. The molecular orbitals of the complex AB in the original atomic orbital basis (atom-centered basis functions) are transformed to the fragment orbital basis set. The transformation matrix contains all of the information that connects the electronic structures of the two fragments, A and B, with that of complex AB. The interpretation of this transformation matrix is simplified in the CDA scheme by partitioning it into terms common to the Dewar−Chatt−Duncanson model: donation (q_d), back-donation (q_b), and repulsive polarization (q_r) between the two fragments. One fragment is defined to be the electron donor fragment, A (for example, a ligand), while the other fragment is the electron acceptor fragment, B (for example, the remaining fragment of the transition-metal complex). The donation term (q_d) is then defined as corresponding to the interaction between the occupied orbitals of the donor fragment A and the unoccupied orbitals of the acceptor fragment B. Back-donation (q_b) arises from the interaction between the occupied orbitals of the electron acceptor fragment B with the unoccupied orbitals of the electron donor fragment A. The repulsive polarization term accounts for the interaction between the occupied orbitals on both fragments. This partitioning is carried out for each MO of the complex, and summing the contributions from all of the MOs yields total amounts of donation, back-donation, and repulsion between the two fragments; e.g., for donation, $q_d = \sum_i q_{d_i}$.

(i) Qualitative Aspects of Bonding. In the present study, the CDA scheme was used as a tool to characterize the nature of the acetylene ligand in both the reactant $M(CO)_4(C_2H_2)$ and CO dissociation product $M(CO)_3(C_2H_2)$. In each complex the acetylene ligand was defined as the electron donor fragment A, and the remaining metal−carbonyl fragment was defined as the electron acceptor B. Table 7 summarizes the total amounts of donation, q_d ($C_2H_2 \rightarrow M$), back-donation, q_b ($C_2H_2 \leftarrow M$), and repulsion, q_r ($C_2H_2 \leftrightarrow M$), for the Fe and Ru analogues of the reactant and CO dissociation product complexes, at the BLYP/BS2//BLYP/BS1 level of theory. Also given in Table 7 are the CDA results for $Ru(CO)_5$ and its corresponding CO dissociation product, $^1A_1$ $Ru(CO)_4$, in which an equatorial carbonyl ligand was defined as the electron donor fragment A and the remaining $Ru(CO)_n$ fragment the electron acceptor fragment B.

Table 7. Summary of Charge Decomposition Analysis[a−c]

			$Fe(CO)_4(C_2H_2)$	$Fe(CO)_3(C_2H_2)$
q_d			0.56	0.72
q_b			0.35	0.51
q_r			−0.37	−0.25
	$Ru(CO)_5$	$Ru(CO)_4$	$Ru(CO)_4(C_2H_2)$	$Ru(CO)_3(C_2H_2)$
q_d	0.30	0.30	0.42	0.62
q_b	0.33	0.29	0.37	0.55
q_r	−0.10	−0.18	−0.32	−0.29

[a] Charge decomposition analysis scheme of Frenking and coworkers.[23] [b] Results shown are for the charge decomposition analysis of the BLYP/BS2 density. [c] In units of electrons.

As seen from Table 7, the loss of an equatorial CO from $Ru(CO)_5$ results in no significant change in the amount of CO→M donation. There is, however, a decrease in the amount of M→CO back-donation, perhaps not surprising since the electron density of the metal in the unsaturated CO dissociation product is expected to decrease upon CO dissociation. In addition there is a substantial increase in the CO↔M repulsion upon CO dissociation, which may reflect the geometrical changes associated with the dissociation.

The loss of a carbonyl from $Fe(CO)_4(C_2H_2)$ and $Ru(CO)_4(C_2H_2)$ leads to an increase in the total amount of donation from the acetylene to the metal fragment by 0.16 and 0.20 electron, respectively, as seen in Table 7. With this increase in donation there is also an increase in the total amount of back-donation from the metal to the acetylene ligand of roughly the same magnitude, perhaps due to the presence of fewer π-acid CO ligands. As intuitively expected, removal of a CO ligand results in a decrease in the repulsion between the acetylene ligand and the metal carbonyl fragment. These results appear to be consistent with the proposed hypothesis of a stabilization of the unsaturated CO dissociation product through an increased donation from the acetylene ligand to the metal. However, there is still no direct evidence for the participation of both π orbitals of the acetylene ligand.

To gain a deeper understanding of the role of the acetylene ligand, especially in the unsaturated $M(CO)_3(C_2H_2)$ intermediate, each of the individual $M-C_2H_2$ MO interactions was analyzed with the CDA scheme. As stated previously, $C_2H_2 \rightarrow M$ bonding can take place through both π orbitals of the acetylene ligand: the $\pi_{||}$ orbital which lies in the equatorial plane and the $\pi_\perp$ orbital which is perpendicular to the equatorial plane. The corresponding antibonding orbitals, $\pi^*_{||}$ and $\pi^*_\perp$, may accept electron density from the metal through back-donation. These four Dewar−Chatt−Duncanson $M-C_2H_2$ interactions, referred to as $\pi-\sigma_d$ ($C_2H_2 \rightarrow M$, $\pi_{||}$), $\pi-\pi_d$ ($C_2H_2 \rightarrow M$, $\pi_\perp$), $\pi^*-\pi_b$ ($M \rightarrow C_2H_2$, $\pi^*_{||}$), and $\pi^*-\delta_b$ ($M \rightarrow C_2H_2$, $\pi^*_\perp$) in the following discussion, are shown in Figures 8 and 9 for the $M(CO)_4(C_2H_2)$ and $M(CO)_3(C_2H_2)$ complexes. As seen in Figure 9a−d it would

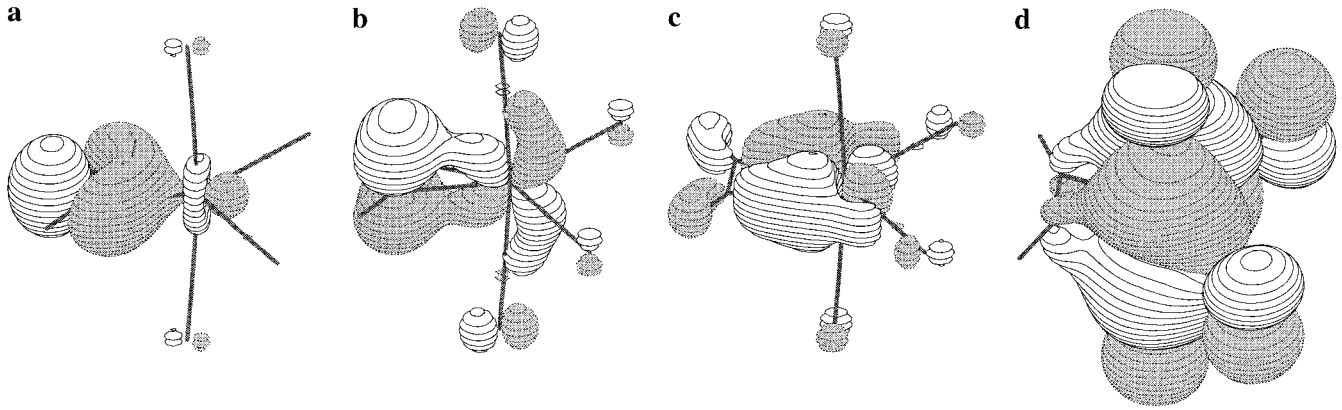

Figure 8. The four Dewar−Chatt−Duncanson type metal−acetylene MO interactions of the saturated $M(CO)_4(C_2H_2)$ complex: (a) $C_2H_2 \rightarrow M$ $\pi_{||}-\sigma$ donation; (b) $C_2H_2 \rightarrow M$ $\pi_{\perp}-\pi$ donation; (c) $C_2H_2 \leftarrow M$ $\pi^*_{||}-\pi$ back-donation; and (d) $C_2H_2 \leftarrow M$ $\pi^*_{\perp}-\delta$ back-donation.

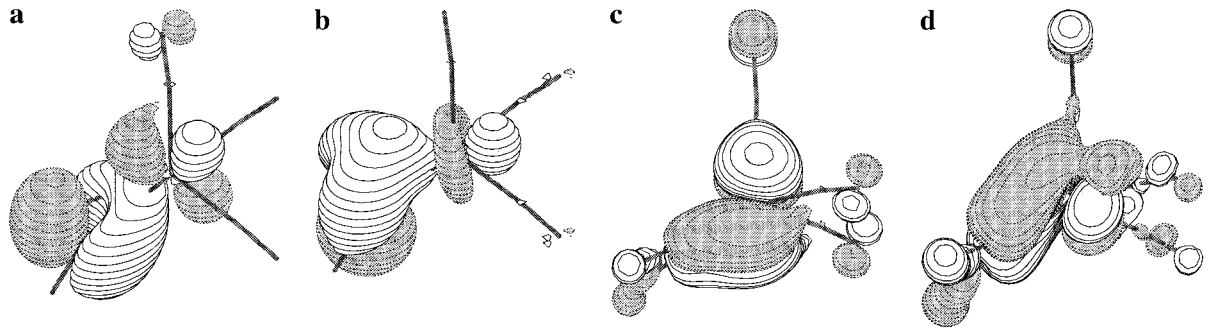

Figure 9. The four Dewar−Chatt−Duncanson type metal−acetylene MO interactions of the unsaturated $M(CO)_3(C_2H_2)$ dissociation product: (a) $C_2H_2 \rightarrow M$ $\pi_{||}-\sigma$ donation; (b) $C_2H_2 \rightarrow M$ $\pi_{\perp}-\pi$ donation; (c) $C_2H_2 \leftarrow M$ $\pi^*_{||}-\pi$ back-donation; and (d) $C_2H_2 \leftarrow M$ $\pi^*_{\perp}-\delta$ back-donation.

Table 8. Charge Decomposition Analysis[a−c] of Metal−Acetylene Bonding in $M(CO)_4(C_2H_2)$ and $M(CO)_3(C_2H_2)$

contribution	$Fe(CO)_4(C_2H_2)$	$Fe(CO)_3(C_2H_2)$[d]	$Ru(CO)_4(C_2H_2)$	$Ru(CO)_3(C_2H_2)$[d]
q_{d_i}, $i = \pi_{||} - \sigma_d$	0.25	0.19	0.17	0.11
q_{d_i}, $i = \pi_{\perp} - \pi_d$	0.02	0.20	0.01	0.14
q_{b_i}, $i = \pi^*_{||} - \pi_b$	0.35	0.20	0.36	0.17
q_{b_i}, $i = \pi^*_{\perp} - \delta_b$	0.00	0.27	0.01	0.33

[a] Charge decomposition analysis scheme of Frenking and co-workers.[23] [b] Results shown are for the charge decomposition analysis of the BLYP/BS2 density. [c] In units of electrons. [d] The orbitals appear to be hybrids in the $M(CO)_3(C_2H_2)$ systems.

appear that the two donor and two back-donor MO interactions in $M(CO)_3(C_2H_2)$ appear to be hybrids of the original MO interactions in the saturated species (Figure 8a−d). The contributions q_{d_i} from the two $C_2H_2 \rightarrow M$ interactions to the CDA donation term, q_d, and the contributions q_{b_i} from the two corresponding $M \rightarrow C_2H_2$ interactions to the back-donation term, q_b, are given in Table 8 for both the Fe and Ru analogues of the saturated and unsaturated alkyne complexes. Since the same bonding picture between the alkyne and the metal emerges for both the Fe and Ru analogues, only the results for the Fe complexes will be discussed in detail. In the formally 18-electron, saturated $Fe(CO)_4(C_2H_2)$ complex only one of the π orbitals, $\pi_{||}$ (i.e. $\pi-\sigma_d$ interaction), is actively involved in donation of electron density to the metal, with a q_{d_i} value of 0.25 electrons. Upon removal of an axial CO, the second acetylene π orbital, $\pi_{\perp}$, becomes an active donor, and donates an equivalent amount of electron density to the metal as the $\pi_{||}$ orbital, with q_{d_i} values of 0.20 and 0.19 electrons respectively. Hence, we see that the role of the acetylene ligand changes along the CO dissociation pathway, going from a two-electron donor in the $Fe(CO)_4(C_2H_2)$ reactant complex to a four-electron donor and thereby stabilizing the CO dissociation product $Fe(CO)_3(C_2H_2)$. Interestingly, a similar picture of back-bonding emerges from the CDA results, with only the $\pi^*_{||}$ orbital accepting electron density from the metal in the reactant complex, while both π^* orbitals actively accept electron density in the CO dissociated $M(CO)_3(C_2H_2)$ complex. In summary, the CDA analysis of the individual Dewar−Chatt−Duncanson $M-C_2H_2$ interactions provides semiquantitative evidence for the hypothesis that it is the participation of both π orbitals of the alkyne that stabilizes the CO dissociated intermediate, thereby leading to reduced CO BDE values with respect to the parent pentacarbonyls. The CDA findings are in full agreement with the structural changes which occur upon CO dissociation.

(ii) Dependence on Basis Set and Molecular Orbitals. The nature of the CDA requires that it be tested for basis set dependence. Dapprich and Frenking conducted some tests for small molecules containg the main-group atoms.[23] In the present work, we performed such an analysis for large systems containing transition-metal elements. The CDA technique was applied to the $Ru(CO)_5$ and $Ru(CO)_4(C_2H_2)$ complexes, at their respective BLYP/BS1 optimized geometries. The corresponding complex and fragment MOs were computed with both RHF and DFT (BLYP functional) methods, in conjunction with the effective core potential basis set (BS1) used in the geometry optimizations, or the all-electron basis set (BS2) used in the AIM analysis. The total values (i.e. summed over all of the MOs of the complex AB) of the CDA terms q_d, q_b, q_r, and q_s (the residual term) are reported in Table 10. In $Ru(CO)_5$, where an equatorial CO was treated as the electron donor fragment

Table 9. Topological Properties at the Bond Critical Points[a] of $M(CO)_5$ and $M(CO)_4(C_2H_2)$ and Their CO Dissociated Products[b,c]

parameter	$\rho(r_c)$	$\nabla^2\rho(r_c)$	$\rho(r_c)$	$\nabla^2\rho(r_c)$
	$Fe(CO)_5$		$Fe(CO)_4(^1A_1)$	
$Fe-C_{ax}$	0.125	0.621	0.133	0.584
$Fe-C_{eq}$	0.132	0.567	0.137	0.589
$C_{ax}-O_{ax}$	0.437	0.518	0.432	0.510
$C_{eq}-O_{eq}$	0.433	0.503	0.430	0.510
	$Fe(CO)_4(C_2H_2)$		$Fe(CO)_3(C_2H_2)$	
$Fe-C_{ax}$	0.124	0.612	0.146	0.650
$Fe-C_{eq}$	0.134	0.601	0.133	0.607
$Fe-C_{ac}$	0.076	0.187	0.122	0.358
$C_{ax}-O_{ax}$	0.437	0.514	0.429	0.467
$C_{eq}-O_{eq}$	0.432	0.479	0.432	0.487
$C_{ac}-C_{ac}$	0.366	−1.108	0.341	−1.008
$C_{ac}-Fe-C_{ac}$[d]	0.075		0.115	
	$Ru(CO)_5$		$Ru(CO)_4$	
$Ru-C_{ax}$	0.117	0.460	0.122	0.444
$Ru-C_{eq}$	0.119	0.425	0.128	0.440
$C_{ax}-O_{ax}$	0.439	0.545	0.436	0.536
$C_{eq}-O_{eq}$	0.434	0.523	0.432	0.506
	$Ru(CO)_4(C_2H_2)$		$Ru(CO)_3(C_2H_2)$	
$Ru-C_{ax}$	0.118	0.459	0.150	0.452
$Ru-C_{eq}$	0.120	0.445	0.123	0.448
$Ru-C_{ac}$	0.075	0.216	0.110	0.305
$C_{ax}-O_{ax}$	0.439	0.540	0.427	0.463
$C_{eq}-O_{eq}$	0.434	0.509	0.433	0.508
$C_{ac}-C_{ac}$	0.364	−1.105	0.342	−1.024
$C_{ac}-Ru-C_{ac}$[d]	0.073		0.103	

[a] Electron density topology analysis via Bader's atoms-in-molecules theory.[25] [b] All of the data given correspond to the topological properties of (3,−1) bond critical points unless otherwise stated. [c] In atomic units. [d] Corresponds to the topological properties of the (3,+1) ring critical point between the C_2H_2 ligand and the metal atom.

Table 10. Method and Basis Set Dependence of the Charge Decomposition Analysis Scheme[a,b]

		method		
		RHF[c]	BLYP[c]	
molecule	CDA term	BS2	BS1	BS2
$Ru(CO)_5$	q_d	0.23	0.39	0.30
	q_b	0.23	0.33	0.33
	q_r	−0.11	−0.07	−0.10
	q_s	−0.04	−0.10	−0.05
$Ru(CO)_4(C_2H_2)$	q_d	−0.06	−0.22	0.42
	q_b	−0.07	0.38	0.37
	q_r	0.05	−0.21	−0.32
	q_s	0.36	−0.61	−0.03

[a] Charge decomposition analysis scheme of Frenking and co-workers.[23] [b] In units of electrons. [c] Densities obtained from single point energy calculations at the respective BLYP/BS1 optimized geometries.

(A), and the remaining $Ru(CO)_4$ fragment the electron acceptor fragment (B), changing from the ECP basis set to the all-electron basis set, within the DFT methodology, results in only minor changes to the values of the CDA terms. Changing methods to RHF, but keeping the same all-electron basis set, again results in reductions of the values of q_d and q_b (by as much as 0.10 electron); however, their relative ratios remain intact, and the same bonding picture arises. So there appears to be only a minor method and basis set dependence of the CDA scheme in the case of the pentacarbonyl. However, the same cannot be said of the alkyne-substituted complex. In $Ru(CO)_4(C_2H_2)$ the effects of method and basis set variation on the CDA terms are more dramatic. The CDA terms calculated with the DFT method in conjunction with the ECP basis set are significantly different from those computed with either the all-electron basis set or the RHF method (in conjunction with the all-electron basis set). When the BLYP/BS1 method is employed the $C_2H_2 \rightarrow M$ donation (q_d) is quite large in magnitude and negative in sign and is accompanied by a large, negative residual term (q_s). Changing to the all-electron basis set yields a positive donation value and a small residual term. CDA results similar to the BLYP/BS1 ones were observed previously by Frenking et al.[20,22] for $WCl_4(C_2H_2)$. They concluded that the acetylene−tungsten bond in these complexes cannot be described according to conventional Dewar−Chatt−Duncanson donor−acceptor interactions, but must be described instead in terms of a metallocyclopropene with shared covalent W−C bonds. Taken at face value, the current CDA results for $Ru(CO)_4(C_2H_2)$ appear to suggest two different modes of bonding between the acetylene ligand and the metal depending on the basis set used. When the ECP basis set (BS1) is employed the CDA results imply that the C_2H_2-Ru bonding is covalent in nature, while it may be considered to be a conventional donor−acceptor interaction when the all-electron basis set (BS2) is employed. Due to the relatively high energy of the excited triplet state of acetylene, estimated to be 82.6 kcal/mol by Schaeffer et al.,[62] and to a lesser degree the moderately high energy of the triplet state of the $Ru(CO)_4$ fragment (our estimate is 16.1 kcal/mol) we believe that the C_2H_2-Ru bonding is more likely of a donor−acceptor nature than of a covalent nature between two excited triplets. The CDA scheme is very useful in its ability to break down the complexity of the wave function or electron density into simple, well-known chemical concepts, but caution should be advised against the tendency to use it as a black-box technique. As has been previously stated by Frenking and co-workers,[21−23] the results of the CDA partitioning scheme are qualitative or semiquantitative in nature, and it is the overall bonding picture that one can extrapolate from the results that is most important, and not the absolute values of the individual terms. Much more work is required to fully understand the dependence of the CDA partitioning scheme on both the basis set functions and molecular orbitals.

2. AIM Results. Bader's atoms-in-molecules (AIM) analysis of the electron density topology was used as a further test of this transition state/product stabilization hypothesis. By using AIM theory the values of the electron density, $\rho(r)$, and the Laplacian of the electron density, $\nabla^2\rho(r)$, at the critical points of the electron density topology (i.e. points where the gradient of the electron density ($\nabla\rho(r)$) is zero) yield information regarding the bonding between the atoms in a molecule. Bader's book[25] provides a detailed discussion of the theory and its practical applications and shows that (1) there exists a correlation between the value of $\rho(r)$ at the (3,−1) bond critical points (BCP) of the topology, denoted as $\rho(r_c)$, and the strength of that particular bond, (2) negative values of $\nabla^2\rho(r_c)$ are indicative of a buildup of electron density, while positive values indicate an area of electron depletion, and (3) relatively small, positive values of $\nabla^2\rho(r_c)$ are typical of closed shell interactions, while values which are large and negative are typical of shared, covalent interactions.

AIM analysis was employed to locate all of the critical points (r_c) of the electron density in the saturated $M(CO)_4(C_2H_2)$ and the formally unsaturated CO dissociated $M(CO)_3(C_2H_2)$ complexes as well as the parent pentacarbonyls and their respective CO dissociated intermediates, at the BLYP/BS2//BLYP/BS1 level of theory. The $\rho(r_c)$ and $\nabla^2\rho(r_c)$ values were then used to gauge the changes in the electron density and the metal−ligand bonding which occur upon CO dissociation. The properties of the bond critical points are summarized in Table

(62) Yamaguchi, Y.; Vacek, G.; Schaeffer, H. F., III *Theor. Chem. Acta* **1993**, *86*, 97.

10. The following discussion will focus on the Fe analogues; however, the same discussion is applicable to the heavier Ru congeners.

In the iron carbonyl complexes, $Fe(CO)_5$ and ($^1A_1$) $Fe(CO)_4$, (3,−1) bond critical points were located along each of the Fe−C and C−O connections. At each of these BCPs, the values of the Laplacian are indicative of closed-shell type interactions. The dissociation of an equatorial CO in $Fe(CO)_5$ causes only minor changes in the properties (<0.01 electron) of the electron density topology. For the alkyne-substituted complexes the electron density topology appears to be more complicated, since not only are (3,−1) BCPs located along each of the Fe−C, C−O, and C−C connections, but also a (3,+1) ring critical point (RCP) was located at the centroid of the metal−acetylene cyclopropene-like ring. As in the parent carbonyls, the $\nabla^2\rho(r_c)$ values at the Fe−C and C−O BCPs are indicative of closed-shell interactions. On the other hand, $\nabla^2\rho(r_c)$ at the C−C and C−H BCPs are negative and relatively large in magnitude and are typical of shared, covalent interactions. CO dissociation from $Fe(CO)_4(C_2H_2)$ results in an increase in the value of $\rho(r_c)$ at the Fe−C_{ax} BCP, while that for the Fe−C_{eq} BCP remains unchanged. The changes in the values of $\rho(r_c)$ at the Fe−C_{ac} and C_{ac}−C_{ac} BCPs are consistent with our structural and CDA findings of an increase in the amount of donation from the acetylene ligand to the metal: $\rho(r_c)$ at the Fe−C_{ac} BCP is increased by 0.03 electron, while that for the C_{ac}−C_{ac} BCP of the acetylene ligand is decreased by the same amount. Even the increase in the $\rho(r_c)$ value at the ring critical point upon CO dissociation is consistent with an increased amount of bonding between the acetylene ligand and the metal. Interestingly, the AIM analysis not only shows the increased C_2H_2→M donation upon dissociation of CO, but it also indicates that this additional electron density appears to be funneled into the bond between the metal atom and the remaining axial carbonyl. In summary, the AIM results are in full agreement with the structural data and CDA findings, and fully support the rationalization of the decrease in CO BDE values of the alkyne-substituted species.

It should be mentioned here that the AIM technique is known to be rather invariant to the choice of basis set and consequently no detailed basis set analysis was carried out.

F. Dependence of the CO BDEs on the Metal Atom. One last item that deserves comment is the marked metal dependence of both the calculated CO BDEs and the experimentally measured $\Delta H^{\ddagger}$ values of the $M(CO)_5$ and $M(CO)_4(C_2H_2)$ systems. The different spin multiplicities of the $M(CO)_4$ ground electronic states make it somewhat difficult to probe the origins of the metal dependence of the parent carbonyls. This is not the case for the alkyne-substituted complexes, as CO dissociation leads to singlet ground states for each metal of the triad. Since the calculated CO BDE values were derived from the total energy difference between the reactant and CO dissociation product complexes, the metal dependence must manifest itself as either a ground-state destabilization effect in the reactant complex or a stabilization effect in the CO dissociation product. Our CDA analysis indicates that it is the participation of the $\pi_\perp$ orbital of the alkyne ligand in the $\pi_\perp$−π_d interaction that stabilizes the formally unsaturated $M(CO)_3(C_2H_2)$ complex, thereby lowering the CO BDE. The CO BDE dependence on the metal may simply reflect a variation in the amount of $\pi_\perp$ C_2H_2→M donation. Hence, we decided to compute the MO energy gap for the interaction between the occupied $\pi_\perp$ orbital of the C_2H_2 ligand and the corresponding unoccupied orbital of correct π symmetry of the $M(CO)_3$ metal fragment, to give an indirect measure of the amount of C_2H_2→M donation. To a first approximation, the smaller the MO energy gap the stronger will be the overlap between the orbitals thereby leading to stronger bonding and more electron density being shifted from the C_2H_2 ligand to the metal. Pictorial representations of the occupied $\pi_\perp$ orbital of the acetylene ligand and the unoccupied $M(CO)_3$ metal fragment orbital of correct π symmetry for overlap are available as Supporting Information. The geometries of the two fragments were kept at their orientations in the $M(CO)_3(C_2H_2)$ complex. The metal dependence of the $\pi_\perp$ C_2H_2→M energy gap in $M(CO)_3(C_2H_2)$, calculated at the BLYP/BS1//BLYP/BS1 level of theory, is reported at the top of Figure 10. The trend in the $\pi_\perp$ C_2H_2→M energy gaps down the triad does indeed match that predicted for the CO BDE values and the experimental $\Delta H^{\ddagger}$ trends, with Fe predicted to have the smallest gap, Ru the largest, and Os an intermediate value. However, upon changing the form of the density functional to B3LYP there is not only an increase in the magnitudes of the MO energy gaps for each metal, but also a significant change in the metal dependence of them. The $\pi_\perp$ C_2H_2→M energy gap for Fe is increased relative to the other two congeners, and it is predicted to be the largest of the triad, followed by Ru and Os. Changing from DFT to ab initio RHF, yet still employing the same basis set, results in a further increase in the magnitudes of the $\pi_\perp$ C_2H_2→M energy gaps for each of the metals as well as a further increase in the gap for Fe relative to that of Ru and Os. It appears that as more Hartree−Fock exchange is incorporated, in going from BLYP to B3LYP to RHF, the magnitude of the $\pi_\perp$ C_2H_2→M energy gap for each of the metals is increased and that for iron is increased relative to the heavier congeners. Hence, the metal dependence of the $\pi_\perp$ MO energy gap varies as the method is changed. These results raise doubts regarding the utility of MO energy gaps in rationalizing chemical phenomena.

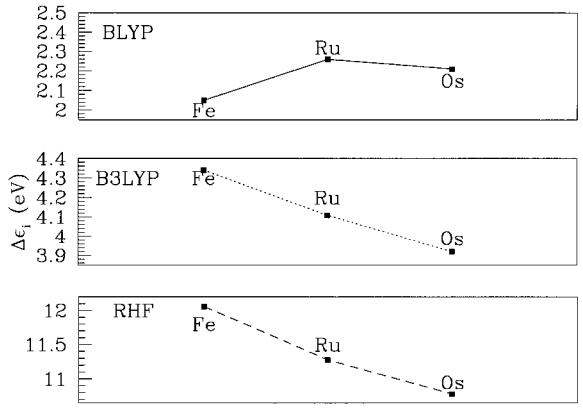

Figure 10. The variation in the computed metal dependence of the C_2H_2→M $\pi_\perp$−π_d energy gap in $M(CO)_3(C_2H_2)$.

4. Conclusions

A variety of nonlocal density functional theory calculations predict a decrease of the first carbonyl dissociation energy of the alkyne-substituted complexes $M(CO)_4(C_2H_2)$ of the iron triad with respect to the parent pentacarbonyl complexes, in full agreement with the results of a recent experimental solution kinetics study. The BLYP optimized geometries of the parent complexes, $M(CO)_5$ and $M(CO)_4(C_2H_2)$, and the CO dissociated products show good agreement with the available experimental data and with the results of previous theoretical studies. Carbonyl dissociation from $Fe(CO)_5$ is predicted to be somewhat complicated by the triplet ground state of the dissociation

product; however, the CO dissociation products of the Ru and Os pentacarbonyls, as well as that of all of the alkyne-substituted complexes, are predicted to have singlet ground states.

With the CDA partitioning scheme, it was shown that the lower CO BDEs of the alkyne-substituted species may be attributed to a stabilization of the formally unsaturated $M(CO)_3(C_2H_2)$ via an increased donation from the acetylene ligand to the metal. In the saturated $M(CO)_4(C_2H_2)$ reactant complex the acetylene ligand is a two-electron donor, with only the $\pi_{\|}$ orbital donating to the metal; on the other hand, in the CO dissociated compound both π orbitals of acetylene donate electron density to the metal, thereby making acetylene formally a four-electron donor and stabilizing the CO dissociated intermediate. The results of the AIM topological analysis of the electron density of the alkyne complexes are in full agreement with the CDA findings. The values of $\rho(r_c)$ at the $M-C_{ac}$ bond critical points increase while those at the $C_{ac}-C_{ac}$ bond critical point decrease upon removal of an axial carbonyl ligand from the Fe and Ru analogues of $M(CO)_4(C_2H_2)$. Even the increase of $\rho(r_c)$ at the M−acetylene ring critical point is consistent with an increase in the amount of bonding between the acetylene ligand and the metal. Furthermore, the structural changes predicted to occur upon CO dissociation were also in accord with the rationale of an increased donation from the alkyne.

Our DFT calculations of the first CO BDEs consistently predict an Fe > Os > Ru metal dependence for the parent pentacarbonyls, and the reverse trend, Fe < Os < Ru, for the alkyne-substituted complexes, in accord with the trends observed experimentally. The different ground states of the $M(CO)_4$ dissociation products complicated analysis of the metal dependence in the parent pentacarbonyls. Simple MO energy gaps for the critical $C_2H_2 \rightarrow M$ $\pi-\pi_d$ interaction, accredited with stabilization of the unsaturated $M(CO)_3(C_2H_2)$ dissociation product, were computed for each metal of the triad. A correlation was found between the $\pi_\perp$ MO energy gaps and the computed CO BDE values when the BLYP density functional was employed. Iron was found to have the smallest MO energy gap, followed by Os and Ru. Upon increasing the amount of HF exchange from BLYP to B3LYP to RHF, the $\pi_\perp$ MO energy gap for Fe increased with respect to Ru and Os, such that it became the largest of the series, in disagreement with the trend predicted for the CO BDEs.

Acknowledgment. All of the calculations were performed on IBM RS/6000 workstations and on the SP2 processor at the University of Alberta. University of Alberta Computing and Network Services are gratefully acknowledged for the use of their computers. This work was partly funded by a research grant from the Natural Sciences and Engineering Research Council of Canada under the Collaborative Special Project Grants Program. S.A.D. would like to thank the Faculty of Graduate Studies at the University of Alberta for a scholarship and the Department of Chemistry for the Harry Emmett Gunning Fellowship. We would also like to thank Dr. Takats and Dr. Jordan and all of the members of their research groups at the University of Alberta for thoughtful discussions. We appreciate careful reading of the manuscript by Dr. Takats. Dr. Frenking and Dr. Dapprich are thanked for the CDA2.1 program as well as for aid in its use.

Supporting Information Available: Tables of selected geometric parameters of $M(CO)_4(C_2H_2)$ and $M(CO)_3(C_2H_2)$ and diagrams of the occupied π MO of the acetylene ligand and the unoccupied π MO of the $M(CO)_3$ metal fragment (6 pages, print/PDF). See any current masthead page for ordering informaiton and Web access instructions.

JA981197M